



# A combined nodal continuous–discontinuous finite element formulation for the Maxwell problem

Santiago Badia <sup>a,\*</sup>, Ramon Codina <sup>b</sup>

<sup>a</sup> Centre Internacional de Metodes Numerics en Enginyeria (CIMNE), Parc Mediterrani de la Tecnologia, Universitat Politècnica de Catalunya, Esteve Terrades 5, 08860 Castelldefels, Spain

<sup>b</sup> Universitat Politècnica de Catalunya, Jordi Girona 1–3, Edifici C1, 08034 Barcelona, Spain

## ARTICLE INFO

### Keywords:

Maxwell's problem  
Electromagnetism  
Finite elements  
Stabilization techniques  
Discontinuous Galerkin methods  
Singular solutions

## ABSTRACT

Continuous Galerkin formulations are appealing due to their low computational cost, whereas discontinuous Galerkin formulation facilitate adaptive mesh refinement and are more accurate in regions with jumps of physical parameters. Since many electromagnetic problems involve materials with different physical properties, this last point is very important. For this reason, in this article we have developed a combined cG–dG formulation for Maxwell's problem that allows arbitrary finite element spaces with functions continuous in patches of finite elements and discontinuous on the interfaces of these patches. In particular, the second formulation we propose comes from a novel continuous Galerkin formulation that reduces the amount of stabilization introduced in the numerical system. In all cases, we have performed stability and convergence analyses of the methods. The outcome of this work is a new approach that keeps the low CPU cost of recent nodal continuous formulations with the ability to deal with coefficient jumps and adaptivity of discontinuous ones. All these methods have been tested using a problem with singular solution and another one with different materials, in order to prove that in fact the resulting formulations can properly deal with these problems.

© 2011 Elsevier Inc. All rights reserved.

## 1. Introduction

The simulation of electromagnetic phenomena increasingly demands more complex geometries and larger scale problems. As an example, Maxwell's equations are in the core of plasma physics and magnetohydrodynamics simulations, coupled with the Vlasov and Navier–Stokes equations respectively. Finite element (FE) methods are a popular approach for the numerical simulation of Maxwell's systems, since realistic geometries can be handled via unstructured grids and can be straightforwardly applied to multi-physics. Furthermore, they possess a strong mathematical foundation that allows one to analyze stability and convergence properties of the algorithms.

Maxwell's equations can be casted in a saddle-point mathematical structure, with the particular feature that the multiplier is zero. With a crude Galerkin formulation, we are enforced to use inf–sup stable FE spaces; for this particular problem, this type of elements are the so-called Nédélec's FEs for the magnetic field and continuous Lagrangian interpolations for the multiplier. Unfortunately, exact penalty formulations that eliminate the Lagrange multiplier from the equations and allow FE spaces that do not satisfy the inf–sup condition lead to spurious solutions (see [17]). In order to rehabilitate the exact penalty formulation, some techniques have been proposed, e.g. the weighted penalty formulation in [17] or the decomposition of singular and smooth parts of the solution in [2,23]. Unfortunately, these approaches require to know where the singularities

\* Corresponding author.

E-mail addresses: [sbadia@cimne.upc.edu](mailto:sbadia@cimne.upc.edu) (S. Badia), [ramon.codina@upc.edu](mailto:ramon.codina@upc.edu) (R. Codina).

will appear (re-entrant corners) and so, are hard to use in an automatic and general way. Very recently, the authors have considered an alternative way to circumvent the inf–sup condition in [4]; see [7] for a related approach. We still consider a saddle-point structure, but now using an equivalent augmented formulation and a stabilized FE discretization of the problem. This way, the resulting method allows one to capture singular solutions for continuous nodal (Lagrangian) FE spaces that do not satisfy the discrete inf–sup condition of the original system. Further, the method is very easy to implement, essentially general and automatically applicable to any problem, without the need to know where the singularities will take place.

Nodal FE approximations are very appealing in terms of CPU cost *versus* accuracy and by the simplicity of data bases (both the solution and Lagrange multiplier can be approximated using the same FE space). Furthermore, they are very effective when considering multi-physics problems, since all the unknowns of the different problems can be solved using the same finite dimensional spaces. For instance, in the magnetohydrodynamics (MHD) problem, the Navier–Stokes equations are often solved using nodal FE stabilization techniques. Analogously, the Vlasov equations in plasma physics can be solved this way. It is clear that this kind of approach greatly simplifies multi-physics codes and monolithic solvers.

However, continuous Lagrangian formulations, onwards denoted as cG, have some drawbacks that can be solved using discontinuous nodal formulations, indicated as dG formulations, that enforce continuity weakly. Examples of dG formulations for Maxwell’s problem can be found in [27,24]. dG approaches are expensive but allow local mesh adaptation and are more accurate in regions in which the solution exhibits jumps, i.e. regions with jumps of physical parameters. Since many electromagnetic problems involve materials with different physical properties, this last point is very important. For this reason, in this article we have developed a combined cG–dG formulation that allows arbitrary FE spaces with functions continuous in patches of FEs and discontinuous on the interfaces of these patches; this is the sense in which the term “combined” is used in this article. This way, we are able to restrict weak continuity to a very reduced number of nodes (e.g. material interfaces or refined regions). As a result, the cG–dG approach shares the low CPU cost of cG formulations with the ability to deal with adaptivity and different materials. Analogously, the coupling of cG and dG methods has been considered in other applications (see, e.g. [26]).

The outline of the paper is as follows. In Section 2 we state the continuous problem and consider different functional settings, as well as the cG formulation in [4] and the dG one in [24]. The combined cG–dG formulation is introduced in Section 3. We have considered two alternative formulations, the second one coming from a new cG formulation based on projections that introduces le numerical dissipation. In all cases, we have performed stability and convergence analyses. Finally, in Section 4 we present some numerical experiments for a problem with singular solution and another one with discontinuous coefficients.

## 2. Problem statement

### 2.1. Notation

Let  $\Omega$  be a bounded domain in  $\mathbb{R}^d$ , with  $d = 2, 3$  the space dimension. Given a Banach space  $X$ , we denote its associated norm by  $\|\cdot\|_X$ ; for the sake of conciseness, we will omit the subscript for  $L^2(\Omega)$ , the space of square integrable functions. The space of vector-valued functions with components in  $X$  is denoted by  $X^d$ . The dimension superscript will be omitted in the norm, i.e. we will simply denote its norm by  $\|\cdot\|_X$  instead of  $\|\cdot\|_{X^d}$ . The dual space of  $X$  is denoted as  $X'$ . The inner product between two scalar or vector functions  $f_1, f_2 \in L^2(\Omega)$  is denoted by  $(f_1, f_2)$ , whereas  $\langle f_1, f_2 \rangle$  is used for a duality pairing in  $X \times X'$  based on the integral.

$W^{s,m}(\Omega)$  is used for the standard Sobolev space, with real coefficients  $s \geq 0$  and  $m \geq 1$ . Hilbert spaces  $W^{s,2}(\Omega)$  are denoted by  $H^s(\Omega)$ . We write  $H_0^1(\Omega)$  for the space of functions in  $H^1(\Omega)$  with null trace on  $\partial\Omega$ . We will make use of the following spaces of vector fields:

$$H(\text{div}; \varepsilon; \Omega) := \left\{ \mathbf{v} \in L^2(\Omega)^d \text{ such that } \nabla \cdot (\varepsilon \mathbf{v}) \in L^2(\Omega) \right\},$$

$$H(\mathbf{curl}; \Omega) := \left\{ \mathbf{v} \in L^2(\Omega)^d \text{ such that } \nabla \times \mathbf{v} \in L^2(\Omega)^d \right\}$$

and the subspaces

$$H(\text{div}_g; \varepsilon; \Omega) := \left\{ \mathbf{v} \in H(\text{div}; \varepsilon; \Omega) \text{ such that } \nabla \cdot (\varepsilon \mathbf{v}) = g \right\},$$

$$H_0(\mathbf{curl}; \Omega) := \left\{ \mathbf{v} \in H(\mathbf{curl}; \Omega) \text{ such that } \mathbf{n} \times \mathbf{v} = \mathbf{0} \text{ on } \partial\Omega \right\},$$

for  $g \in L^2(\Omega)$  and  $\varepsilon$  a piecewise function on  $\Omega$  (see below). We use the notation  $A \lesssim B$  to indicate that  $A \leq C B$ , where  $A$  and  $B$  are expressions depending on functions that in the discrete case may depend on the discretization as well, and  $C$  is a positive constant.

### 2.2. The continuous problem

We consider the Maxwell problem, which physically describes magnetostatics and electrostatics in a bounded domain  $\Omega$  surrounded by a perfect conductor. Let us consider  $\Omega \subset \mathbb{R}^d$  to be a simply connected in general non-convex polyhedral

domain with a connected Lipschitz continuous boundary  $\partial \Omega$ . Besides its range of applicability, this system of partial differential equations exhibits the mathematical complications encountered in more involved model problems (see, e.g. [19,11]). Maxwell's problem can be stated as a saddle-point problem by enforcing the divergence constraint with a Lagrange multiplier  $p$ . The Euler–Lagrange equations read as follows: seek a pair  $(\mathbf{u}, p)$  solution of

$$\nabla \times (\lambda \nabla \times \mathbf{u}) - \varepsilon \nabla p = \mathbf{f}, \quad (1a)$$

$$-\nabla \cdot (\varepsilon \mathbf{u}) = g \quad (1b)$$

for some divergence-free datum  $\mathbf{f}$ . We assume that the physical properties  $\lambda(\mathbf{x}) > 0$  and  $\varepsilon(\mathbf{x}) > 0$  are piecewise constant functions since this is the case of interest, i.e.  $\Omega$  is filled with different materials. For the electrostatic problem,  $\mathbf{u}$  is the electric field,  $\mathbf{f}$  is equal to zero,  $\varepsilon$  is the electric permittivity and  $\lambda = 1$ . The problem is supplemented with the homogeneous boundary conditions  $\mathbf{n} \times \mathbf{u} = \mathbf{0}$  and  $p = 0$  on  $\partial \Omega$ . On the other hand, for the magnetostatic problem,  $\mathbf{u}$  is the magnetic field,  $g = 0$ ,  $\varepsilon$  is the magnetic permeability and  $\lambda = 1$ . The homogeneous boundary condition in this case reads  $\mathbf{n} \times \nabla \times \mathbf{u} = \mathbf{0}$  and  $\mathbf{n} \cdot \mathbf{u} = 0$  (see, e.g. [23]); zero mean value for  $p$  must be enforced to make the problem well-posed. This problem is also encountered when solving magnetostatics in terms of the magnetic vector potential with Coulomb's gauge  $\nabla \cdot \mathbf{u} = 0$ ;  $\lambda$  is the inverse of the magnetic permeability and  $\varepsilon = 1$  in this case. Anyway, for the generalization to the time-dependent Maxwell equations, we must work with arbitrary  $(\lambda, \varepsilon)$ .

In the sequel, let us consider  $(\lambda, \varepsilon)$  to be the dimensionless relative values with respect to the ones for the vacuum  $(\lambda_0, \varepsilon_0)$ , i.e.  $(\lambda, \varepsilon) \leftarrow (\lambda/\lambda_0, \varepsilon/\varepsilon_0)$ . The scaled system is obtained after multiplying (1a) and (1b) against  $1/\lambda_0$  and  $1/\varepsilon_0$ , respectively, and properly re-defining  $p \leftarrow \varepsilon_0 p/\lambda_0$ ,  $\mathbf{f} \leftarrow \mathbf{f}/\lambda_0$  and  $g \leftarrow g/\varepsilon_0$ .

Formally taking the divergence of (1a), we obtain  $-\Delta p = \nabla \cdot \mathbf{f} = 0$ . Invoking the boundary conditions in the electrostatic case or the zero mean value in the magnetostatic one, we finally prove that  $p = 0$ .

The variational interpretation of the mixed problem (1) admits two functional settings. The so-called curl formulation reads as: find  $\mathbf{u} \in H_0(\mathbf{curl}; \Omega)$  and  $p \in H_0^1(\Omega)$  such that

$$(\lambda \nabla \times \mathbf{u}, \nabla \times \mathbf{v}) - (\varepsilon \nabla p, \mathbf{v}) = (\mathbf{f}, \mathbf{v}), \quad \forall \mathbf{v} \in H_0(\mathbf{curl}; \Omega), \quad (2a)$$

$$(\varepsilon \nabla q, \mathbf{u}) = (g, q), \quad \forall q \in H_0^1(\Omega), \quad (2b)$$

where  $\mathbf{f} \in H(\text{div}_0; \Omega)$  (space of divergence free vector fields) is assumed. However, this is not the only functional setting in which the problem is well-posed; the  $H^1(\Omega)$  regularity for  $p$  can be “transferred” to  $\mathbf{u}$ , leading to a curl–div variational formulation: find  $\mathbf{u} \in H_0(\mathbf{curl}; \Omega) \cap H(\text{div}; \varepsilon; \Omega)$  and  $p \in L^2(\Omega)/\mathbb{R}$  such that

$$(\lambda \nabla \times \mathbf{u}, \nabla \times \mathbf{v}) + (p, \nabla \cdot (\varepsilon \mathbf{v})) = (\mathbf{f}, \mathbf{v}), \quad \forall \mathbf{v} \in H_0(\mathbf{curl}; \Omega) \cap H(\text{div}; \varepsilon; \Omega), \quad (3a)$$

$$-(q, \nabla \cdot (\varepsilon \mathbf{u})) = (g, q), \quad \forall q \in L^2(\Omega). \quad (3b)$$

On the other hand, since  $p = 0$ , the curl–div formulation can be equivalently written as an exact penalty method: seek  $\mathbf{u} \in H_0(\mathbf{curl}; \Omega) \cap H(\text{div}; \varepsilon; \Omega)$  such that

$$(\lambda \nabla \times \mathbf{u}, \nabla \times \mathbf{v}) + (\nabla \cdot (\varepsilon \mathbf{u}), \nabla \cdot (\varepsilon \mathbf{v})) = (\mathbf{f}, \mathbf{v}) - (g, \nabla \cdot (\varepsilon \mathbf{v})), \quad (4)$$

for any  $\mathbf{v} \in H_0(\mathbf{curl}; \Omega) \cap H(\text{div}; \varepsilon; \Omega)$ . The equivalence between these three formulations can be found, e.g. in [22]. At the discrete level, however, these formulations lead to methods with quite different properties. A deep mathematical analysis of the singularities that appear with discontinuous coefficients can be found in [18].

In the curl formulation (2), let us denote by  $V$  the space  $H_0(\mathbf{curl}; \Omega)$  for the solution  $\mathbf{u}$  and by  $Q$  the space  $H_0^1(\Omega)$  for the Lagrange multiplier  $p$ . Furthermore, let us write (2) in compact form as

$$c(\mathbf{u}, p, \mathbf{v}, q) = (\mathbf{f}, \mathbf{v}) + (g, q) \quad \text{where} \quad c(\mathbf{u}, p, \mathbf{v}, q) = (\lambda \nabla \times \mathbf{u}, \nabla \times \mathbf{v}) - (\varepsilon \nabla p, \mathbf{v}) + (\varepsilon \nabla q, \mathbf{u}).$$

In [4], the authors have proposed a novel numerical approximation of the Maxwell problem whose starting point is a different augmented formulation of the continuous problem. Since we are interested in a curl formulation for reasons that will be explained later on, we add the term  $\ell^2 \nabla \cdot (\varepsilon \nabla p)$  to (1b);  $\ell > 0$  has dimensions of length, and it has been introduced in order to end up with a dimensionally consistent method. A length scale is inherent to the problem, since it is needed to define dimensionally consistent norms for these spaces, which are given by

$$\|\mathbf{v}\|_V := \|\mathbf{v}\|_{H(\mathbf{curl}; \Omega)} = \frac{1}{\ell} \|\mathbf{v}\| + \|\nabla \times \mathbf{v}\|, \quad (5)$$

$$\|q\|_Q := \|q\|_{H_0^1(\Omega)} = \frac{1}{\ell} \|q\| + \|\nabla q\|, \quad (6)$$

where  $\ell = \ell(\Omega)$  makes the norms dimensionally consistent. Theoretically, this length scale comes from the Poincaré–Friedrichs inequality of the problem at hand. The augmented formulation in strong form consists of finding  $\mathbf{u}$  and  $p$  such that

$$\nabla \times (\lambda \nabla \times \mathbf{u}) - \varepsilon \nabla p = \mathbf{f}, \quad (7a)$$

$$-\nabla \cdot (\varepsilon \mathbf{u}) - \ell^2 \nabla \cdot (\varepsilon \nabla p) = g, \quad (7b)$$

in  $\Omega$ , satisfying  $\mathbf{n} \times \mathbf{u} = \mathbf{0}$  and  $p = 0$  on  $\partial\Omega$ . Since  $p \in Q$  is identically zero, the penalty is exact. The equivalence of the new formulation (7) and (2) can be found in [4].

### 2.3. Numerical approximation

Although all the formulations introduced above are equivalent, stable and consistent, numerical approximations of the curl-div formulations (3) and (4) lead to spurious solutions for nonconvex domains, e.g. domains with re-entrant corners. Costabel provided in [15] a mathematical justification to this surprising observation: since  $\Omega$  is not convex,  $V \cap H^1(\Omega)^d$  is a closed proper subspace of  $V \cap H(\text{div}; \Omega)$ . One could think that a  $H^1$ -conforming FE space cannot be used, since the FE space is a closed proper subspace of  $V \cap H(\text{div}; \Omega)$  and the FE solution  $\mathbf{u}_h$  can be shown to be bounded in  $H^1(\Omega)^d$  (see, e.g. [22] or [20, Corollary 2.30]). However, this reasoning is wrong in general. The approximability lost only happens when the sequence of solutions  $\{\mathbf{u}_h\}_{h>0}$  is uniformly bounded in  $H^1(\Omega)^d$ , which is only true for curl-div formulations (see [4, Corollary 1]). Therefore, approximations based on (3) and (4) cannot capture solutions  $\mathbf{u} \notin V \cap H^1(\Omega)^d$  of the Maxwell problem (2), and so, are not suitable for numerical purposes. This kind of solutions are called *nonsmooth* or *singular* solutions. Note that the key for this negative result is the spurious control on the divergence of the approximations based on (3) and (4), which implies that the whole gradient is uniformly bounded in  $L^2(\Omega)$ , since  $\mathbf{u}_h$  is a  $H^1(\Omega)^d$  function for all  $h$ . It is *not* an approximability problem of FE spaces  $V_h \subset H^1(\Omega)^d$  for  $h$  fixed, which may well approximate  $H(\text{curl}; \Omega)$ , as we will see later. These FE spaces are dense not only in  $H(\text{curl}; \Omega)$ , but also in  $L^2(\Omega)^d$ .

On the other hand, the problem (2) in the good functional setting, with a crude Galerkin discretization can only be used with inf-sup stable elements satisfying:

$$\inf_{(\mathbf{u}_h, p_h) \in V_h \times Q_h \setminus \{0,0\}} \sup_{(\mathbf{v}_h, q_h) \in V_h \times Q_h \setminus \{0,0\}} \frac{c(\mathbf{u}_h, p_h; \mathbf{v}_h, q_h)}{\|(\mathbf{u}_h, p_h)\|_{V \times Q} \|(\mathbf{v}_h, q_h)\|_{V \times Q}} \geq \beta_d > 0 \tag{8}$$

for  $\beta_d > 0$  uniform with respect to  $h$  (see, e.g. [9]). This is satisfied by  $V_h$  built by the celebrated Nédélec’s (or edge) elements; those elements are only conforming in  $H(\text{curl}; \Omega)$ , since they do not satisfy normal continuity over the element faces. A nodal FE space can be used for  $Q_h$  (see, e.g. [28]).

In the next, we consider an alternative nodal (Lagrangian) FE approach to this problem, that can circumvent (8). It is motivated by the augmented formulation (7).

#### 2.3.1. Finite element notation

Let  $\mathcal{T}_h$  be a partition of  $\Omega$  into a set of FEs  $\{K\}$ . For every element  $K$ , we denote by  $h_K$  its diameter, and set the characteristic mesh size as  $h = \max_{K \in \mathcal{T}_h} h_K$ . We denote by  $h_I$  the piecewise constant function that takes the value  $h_K$  at every element  $K \in \mathcal{T}_h$ . For simplicity, we consider a regular and quasi-uniform family  $\{\mathcal{T}_h\}_{h>0}$  of FE partitions. The space of polynomials of degree less or equal to  $k > 0$  in a FE  $K$  is denoted by  $\mathcal{P}_k(K)$ . Summation over all the elements will be indicated by  $\sum_K$  and the broken integral  $\sum_K \int_K$  will be denoted by  $\int_{\mathcal{T}_h}$ .

Suppose now that elements  $K_1$  and  $K_2$  share a face (edge)  $E$ , and let  $\mathbf{n}_1$  and  $\mathbf{n}_2$  be the normals to  $E$  exterior to  $K_1$  and  $K_2$ , respectively. For a scalar function  $f$ , possibly discontinuous across  $E$ , we define its jump and average as

$$\begin{aligned} \llbracket f \rrbracket &:= \mathbf{n}_1 f|_{\partial K_1 \cap E} + \mathbf{n}_2 f|_{\partial K_2 \cap E}, \\ \{f\} &:= \frac{1}{2} (f|_{\partial K_1 \cap E} + f|_{\partial K_2 \cap E}), \end{aligned}$$

whereas for vectorial quantities we will use

$$\begin{aligned} \llbracket \mathbf{v} \rrbracket &:= \mathbf{n}_1 \cdot \mathbf{v}|_{\partial K_1 \cap E} + \mathbf{n}_2 \cdot \mathbf{v}|_{\partial K_2 \cap E}, \quad \llbracket \mathbf{v} \rrbracket_t := \mathbf{n}_1 \times \mathbf{v}|_{\partial K_1 \cap E} + \mathbf{n}_2 \times \mathbf{v}|_{\partial K_2 \cap E}, \\ \{\mathbf{v}\} &:= \frac{1}{2} (\mathbf{v}|_{\partial K_1 \cap E} + \mathbf{v}|_{\partial K_2 \cap E}). \end{aligned}$$

We extend these definitions on  $\partial\Omega$  as  $\llbracket f \rrbracket := \mathbf{n} f$  and  $\{f\} := f$  and similarly for vector functions. Further, let us define the mesh size  $h_\perp$  (defined over the set of faces of the mesh) that on  $E$  takes the value  $h_\perp := (\mathbf{x}_{b_2} - \mathbf{x}_{b_1}) \cdot \mathbf{n}_1 > 0$ , where  $\mathbf{x}_{b_2}$  and  $\mathbf{x}_{b_1}$  are the barycentric coordinates of elements  $K_1$  and  $K_2$ .

The space of discontinuous piecewise polynomials of order  $k > 0$  is defined as

$$\mathcal{H}_k(\Omega) := \left\{ v_h \in L^2(\Omega) \text{ such that } v_h|_K \in \mathcal{P}_k(K) \ \forall K \in \mathcal{T}_h \right\}. \tag{9}$$

Any function in  $\mathcal{H}_k(\Omega)$  can be uniquely determined by its values on a set of points (nodes) in  $\Omega$  (see [8,20]), and so this is a nodal FE approximation. Continuous FE spaces are denoted as  $\mathcal{N}_k := \mathcal{H}_k \cap C^0(\Omega)$ , where  $C^0(\Omega)$  is the space of continuous functions in  $\Omega$ . These approximations are usually called  $H^1$ -conforming approximations since, because of the inter-element continuity, functions in  $\mathcal{N}_k$  are  $H^1$  for each fixed  $h$ .

For quasi-uniform partitions, there is a constant  $C_{\text{inv}}$ , independent of the mesh size  $h$  (the maximum of all the element diameters), such that

$$\|\nabla v_h\|_{L^2(K)} \leq C_{\text{inv}} h^{-1} \|v_h\|_{L^2(K)}, \quad (10)$$

$$\|\Delta v_h\|_{L^2(K)} \leq C_{\text{inv}} h^{-1} \|\nabla v_h\|_{L^2(K)} \quad (11)$$

for all FE functions  $v_h$  defined on  $K \in \mathcal{T}_h$ . This inequality can be used for scalars, vectors or tensors. Similarly, the trace inequality

$$\|v\|_{L^2(\partial K)}^2 \leq C_{\text{tr}} \left( h^{-1} \|v\|_{L^2(K)}^2 + h \|\nabla v\|_{L^2(K)}^2 \right) \quad (12)$$

is assumed to hold for functions  $v \in H^1(K)$ ,  $K \in \mathcal{T}_h$ . If  $\psi_h$  is a piecewise (continuous or discontinuous) polynomial, the last term in the previous inequality can be dropped using an inverse inequality, getting  $\|\psi_h\|_{L^2(\partial K)}^2 \lesssim h^{-1} \|\psi_h\|_{L^2(K)}^2$ .

### 2.3.2. A cG nodal solver

For the reasons explained above, nodal elements have traditionally been related to curl–div conforming formulations, whereas edge elements have been related to curl formulations. In [4] the authors claim that this correspondence is false. So, they propose a stabilized FE formulation based on the augmented formulation (7), which is stated in the curl setting and does not require to satisfy (8) for stability purposes. In fact, the resulting method is stable for any pair of Lagrangian FE spaces.

The cG method in [4] can be motivated as a residual-based stabilized discretization of the exact augmented formulation (7). Let us consider nodal FE approximations  $V_h = \mathcal{N}_k^d \cap V$  and  $Q_h = \mathcal{N}_l/\mathbb{R}$  of the continuous spaces  $V$  and  $Q$ , respectively;  $k, l > 0$  are the orders of approximation for  $\mathbf{u}$  and  $p$ , respectively; there is no restriction between  $k$  and  $l$ , and equal-order approximations are allowed. The method consists of seeking  $\mathbf{u}_h \in V_h$  and  $p_h \in Q_h$  solution of

$$(\lambda \nabla \times \mathbf{u}_h, \nabla \times \mathbf{v}_h) - (\varepsilon \nabla p_h, \mathbf{v}_h) + s_u(\mathbf{u}_h, \mathbf{v}_h) = (\mathbf{f}, \mathbf{v}_h), \quad \forall \mathbf{v}_h \in V_h, \quad (13a)$$

$$(\varepsilon \nabla q_h, \mathbf{u}_h) + s_p(p_h, q_h) = (\mathbf{g}, q_h), \quad \forall q_h \in Q_h, \quad (13b)$$

where the stabilization terms read:

$$s_u(\mathbf{u}_h, \mathbf{v}_h) = \frac{c_u}{\ell^2} \int_{\mathcal{T}_h} \frac{h_l^2}{\varepsilon} \nabla \cdot (\varepsilon \mathbf{u}_h) \nabla \cdot (\varepsilon \mathbf{v}_h), \quad s_p(p_h, q_h) = \ell^2 \int_{\mathcal{T}_h} \varepsilon \nabla p_h \cdot \nabla q_h, \quad (14)$$

$c_u$  being an algorithmic constant. The reason why the term  $s_u$  is needed becomes evident from both theoretical analysis and numerical experimentation. Obviously, as  $h \rightarrow 0$  this term vanishes, and the method is not a curl–div conforming algorithm. Furthermore, in order to have optimal convergence properties, the mesh must be processed, in order to get a macro-element structure (see [4] and Section 3.1).

We can easily see that (13) is a residual-based FE approximation of the augmented formulation (7) (see, e.g. [25,13]). However, it has been observed in [3] that also the multiplier stabilization term can be motivated as a residual-based stabilization term, and so, it does not require to pass through the augmented formulation (see Remark 3.1). This interpretation is appealing for multi-physics problems, since residual-based stabilized formulations are available for the Navier–Stokes and Darcy equations, and a unified framework for all these problems can be considered.

At the same time [4] was written, Bonito and Guermond proposed in [7] a formulation for the more complicated Maxwell eigenvalue problem that, when restricted to the boundary value problem, leads to a very similar method. The only difference is the fact that the method they proposed used

$$s_u(\mathbf{u}_h, \mathbf{v}_h) = \int_{\mathcal{T}_h} h_l^{2\alpha} \nabla \cdot \mathbf{u}_h \nabla \cdot \mathbf{v}_h, \quad \text{for } \alpha \in \left(\frac{1}{2}, 1\right)$$

and no macro-element mesh typology was enforced. For  $\alpha = 1$  the method is identical to the one in [4]. However, the analysis in [7, Theorem 5.1] does not provide any convergence result for  $\alpha = 1$  while the analysis in [4] leads to optimal convergence estimates under the assumption that the mesh has a particular macro-element structure. Numerical experiments included in Section 4 show that this macro-element structure is not just a theoretical artifact. With an appropriate macro-element mesh typology, the method clearly improves the error and the convergence order for the singular corner solution with respect to those obtained in an arbitrary mesh.

### 2.3.3. A dG nodal solver

Nodal dG formulations for the Maxwell problem have been proposed, e.g. in [27,24]. The method in [27] included some terms that were not essential and were eliminated in the more recent formulation [24]. This last formulation is based on an interior penalty dG approximation of the Maxwell problem in the curl setting (2). For the sake of brevity, we just indicate in the next section the terms in the combined cG–dG formulation that have to be eliminated to recover the dG formulation in [24]. Further details in the motivation of the method and its numerical analysis can be found in the original paper. Let us remark that the method proposed in [24] is only suitable for equal-order approximations of  $\mathbf{u}$  and  $p$ , whereas any approximation order can be used with our approach.

### 3. The combined cG–dG formulation

#### 3.1. First formulation of the method

We consider an agglomeration of the triangulation  $\mathcal{T}_h$  into a set of  $n_p$  patches. Let  $\mathcal{S}_h$  be the partition of  $\Omega$  into patches. We assume that the agglomeration is such that every patch  $S \in \mathcal{S}_h$  is connected. At this point, we can define the set of FE functions in the combined cG–dG formulation as follows: we denote the cG–dG nodal FE space of order  $k$  as

$$\begin{aligned} \mathcal{M}_k(\mathcal{S}_h, \mathcal{T}_h) &:= \{v_h \in L^2(\Omega) \text{ such that } v_h|_K \in \mathcal{P}_k(K), \forall K \in \mathcal{T}_h, \\ &\text{and } v_h|_S \in \mathcal{C}^0(S), \forall S \in \mathcal{S}_h\}. \end{aligned}$$

We simply denote this finite dimensional space as  $\mathcal{M}_k$  for the sake of conciseness. Let us indicate by  $\mathcal{F}_h := \cup_{S \in \mathcal{S}_h} \partial S$  the set of patch interfaces (faces or edges), whereas the interior interfaces are denoted by  $\mathcal{F}_h^0 := \mathcal{F}_h \setminus \partial\Omega$ . The  $L^2$  norm over the manifold  $\mathcal{F}_h$  is denoted by  $\|\cdot\|_{\mathcal{F}_h}$ , and analogously for  $\mathcal{F}_h^0$ . We also denote the broken integral over the patches as  $\int_{\mathcal{S}_h}(\cdot) := \sum_{S \in \mathcal{S}_h} \int_S(\cdot)$ . The broken norm over  $\mathcal{S}_h$  is denoted by  $\|\cdot\|_{\mathcal{S}_h}$ . Limit cases in this approach are the dG case in which there is no agglomeration, i.e. every FE domain becomes a patch ( $\mathcal{S}_h = \mathcal{T}_h$ ), and the cG case in which there is only one patch ( $\mathcal{S}_h = \{\Omega\}$ ).

The motivation of the patches is to allow discontinuities on their interfaces. So, the choice of patches must be such that the physical parameters  $(\lambda, \varepsilon)$  are constant inside every patch  $S \in \mathcal{S}_h$ , i.e. two different materials cannot be included in the same patch.

We can easily check that the proposed nodal cG approach cannot be straightforwardly used with  $\mathcal{M}_k$ , since  $\mathcal{C}^0$  continuity has been assumed in its design. On the other hand, a dG formulation is not stable when the unknowns are continuous in patches, because it assumes inclusions between the FE pairs for  $\mathbf{u}_h$  and  $p_h$  that are not true in general. So, a stable cG–dG formulation requires to combine the stable nodal formulation in [4] with an effective dG formulation (e.g. the one in [24]) in a suitable way.

The cG–dG method we propose is designed starting with the cG nodal formulation and adding the corresponding boundary terms on  $\mathcal{F}_h$ . It is well-known that it is not enough with the additional terms that appear after integration-by-parts, and stabilizing jump terms have to be added; we refer to [1] for a detailed exposition of different approaches. In particular, we use an interior penalty stabilization, since this is the approach used in [24]. Let us pick  $V_h = (\mathcal{M}_k)^d$  and  $Q_h = \mathcal{M}_l$ ; we consider the general case in which different approximation orders can be used for the different unknowns.

Let us motivate the jump terms, for the sake of completeness. Integrating by parts  $\nabla \times (\lambda \nabla \times \mathbf{u})$  for  $\mathbf{u}$  the exact solution, against a function  $\mathbf{v}_h \in V_h$ , we have:

$$\begin{aligned} \int_{\Omega} \mathbf{v}_h \cdot \nabla \times (\lambda \nabla \times \mathbf{u}) &= \int_{\mathcal{S}_h} \nabla \times \mathbf{v}_h \cdot \lambda \nabla \times \mathbf{u} - \sum_S \int_{\partial S} \mathbf{n} \times \mathbf{v}_h \cdot \lambda \nabla \times \mathbf{u} \\ &= \int_{\mathcal{S}_h} \nabla \times \mathbf{v}_h \cdot \lambda \nabla \times \mathbf{u} - \int_{\mathcal{F}_h} \llbracket \mathbf{v}_h \rrbracket_t \cdot \{\lambda \nabla \times \mathbf{u}\} - \sum_S \int_{\partial S} \mathbf{n} \times \{\mathbf{v}_h\} \cdot \lambda \nabla \times \mathbf{u} \\ &= \int_{\mathcal{S}_h} \nabla \times \mathbf{v}_h \cdot \lambda \nabla \times \mathbf{u} - \int_{\mathcal{F}_h} \llbracket \mathbf{v}_h \rrbracket_t \cdot \{\lambda \nabla \times \mathbf{u}\} - \int_{\mathcal{F}_h} \llbracket \mathbf{u} \rrbracket_t \cdot \{\lambda \nabla \times \mathbf{v}_h\}, \end{aligned} \tag{15}$$

after invoking the continuity of the solution and its flux. Using a typical dG formulation, the gradient term may be written as

$$\int_{\Omega} \varepsilon \nabla p \cdot \mathbf{v}_h = \int_{\mathcal{S}_h} \varepsilon \nabla p \cdot \mathbf{v}_h - \int_{\mathcal{F}_h} \llbracket p \rrbracket \cdot \{\varepsilon \mathbf{v}_h\}, \tag{16}$$

whereas the divergence term reads as:

$$\int_{\Omega} q_h \nabla \cdot (\varepsilon \mathbf{u}) = - \int_{\mathcal{S}_h} \varepsilon \nabla q_h \cdot \mathbf{u} + \int_{\mathcal{F}_h} \llbracket q_h \rrbracket \cdot \{\varepsilon \mathbf{u}\}. \tag{17}$$

A new term that comes from the proposed augmented formulation and does not appear in [24] is the multiplier Laplacian. We have:

$$- \int_{\Omega} q_h \nabla \cdot (\varepsilon \nabla p) = \int_{\mathcal{S}_h} \varepsilon \nabla q_h \cdot \nabla p - \int_{\mathcal{F}_h} \llbracket q_h \rrbracket \cdot \{\varepsilon \nabla p\} - \int_{\mathcal{F}_h} \llbracket \varepsilon \nabla p \rrbracket \{q_h\} = \int_{\mathcal{S}_h} \varepsilon \nabla q_h \cdot \nabla p \tag{18}$$

where we have deleted the boundary terms, since  $p = 0$  and they are only effective for consistency but not for stability purposes. Finally, in order to prove stability in the appropriate broken norms to be defined, we will introduce to the final bilinear form of the problem the interior penalty stabilizing terms:

$$c_{tu} \int_{\mathcal{F}_h} \frac{\{\lambda\}}{h_{\perp}} \llbracket \mathbf{u}_h \rrbracket_t \cdot \llbracket \mathbf{v}_h \rrbracket_t + \frac{c_{nu}}{\ell^2} \int_{\mathcal{F}_h^0} \frac{h_{\perp}}{\{\varepsilon\}} \llbracket \varepsilon \mathbf{u}_h \rrbracket \llbracket \varepsilon \mathbf{v}_h \rrbracket + c_{np} \ell^2 \int_{\mathcal{F}_h} \frac{\{\varepsilon\}}{h_{\perp}} \llbracket p_h \rrbracket \cdot \llbracket q_h \rrbracket,$$

where  $c_{tu}$ ,  $c_{nu}$  and  $c_{np}$  are algorithmic constants.

Combining the cG approach (13a)-(13b) with the dG strategy described, the cG–dG formulation we propose reads as follows: find  $\mathbf{u}_h \in V_h$  and  $p_h \in Q_h$  such that

$$a_h(\mathbf{u}_h, \mathbf{v}_h) - b_h(p_h, \mathbf{v}_h) = (\mathbf{f}, \mathbf{v}_h), \quad \text{for any } \mathbf{v}_h \in V_h, \tag{19a}$$

$$b_h(q_h, \mathbf{u}_h) + s_h(p_h, q_h) = (g, q_h), \quad \text{for any } q_h \in Q_h, \tag{19b}$$

where the discrete forms have the expressions:

$$\begin{aligned} a_h(\mathbf{u}_h, \mathbf{v}_h) &:= \int_{S_h} \lambda \nabla \times \mathbf{v}_h \cdot \nabla \times \mathbf{u}_h - \int_{\mathcal{F}_h} \llbracket \mathbf{v}_h \rrbracket_t \cdot \{\lambda \nabla \times \mathbf{u}_h\} - \int_{\mathcal{F}_h} \llbracket \mathbf{u}_h \rrbracket_t \cdot \{\lambda \nabla \times \mathbf{v}_h\} \\ &\quad + c_{tu} \int_{\mathcal{F}_h} \frac{\{\lambda\}}{h_\perp} \llbracket \mathbf{u}_h \rrbracket_t \cdot \llbracket \mathbf{v}_h \rrbracket_t + \frac{c_u}{\ell^2} \int_{\mathcal{T}_h} \frac{h_l^2}{\varepsilon} \nabla \cdot (\varepsilon \mathbf{u}_h) \nabla \cdot (\varepsilon \mathbf{v}_h) + \frac{c_{nu}}{\ell^2} \int_{\mathcal{F}_h^0} \frac{h_\perp}{\{\varepsilon\}} \llbracket \varepsilon \mathbf{u}_h \rrbracket \llbracket \varepsilon \mathbf{v}_h \rrbracket, \\ b_h(p_h, \mathbf{v}_h) &:= \int_{S_h} \varepsilon \nabla p_h \cdot \mathbf{v}_h - \int_{\mathcal{F}_h} \llbracket p_h \rrbracket \cdot \{\varepsilon \mathbf{v}_h\}, \\ s_h(p_h, q_h) &:= \ell^2 \int_{S_h} \varepsilon \nabla p_h \cdot \nabla q_h + c_{np} \ell^2 \int_{\mathcal{F}_h} \frac{\{\varepsilon\}}{h_\perp} \llbracket p_h \rrbracket \cdot \llbracket q_h \rrbracket. \end{aligned} \tag{20}$$

**Remark 3.1.** The grad-grad term in (18) can also be motivated as a residual-based stabilization term of streamline-upwind Petrov–Galerkin type (see [3]) with stabilization parameter  $\varepsilon^{-1}$ , since:

$$(\nabla \times (\lambda \nabla \times \mathbf{u}) - \varepsilon \nabla p - \mathbf{f}, \nabla q) = (\varepsilon \nabla p, \nabla q).$$

**Remark 3.2.** In the most general case in which we consider a non-solenoidal forcing term  $\mathbf{f}$ , we can still use the previous formulation. In this case, the multiplier  $p$  is no longer zero, in general. Instead, it satisfies  $-\nabla \cdot (\varepsilon \nabla p) = \nabla \cdot \mathbf{f}$ , which is obtained taking the divergence of Eq. (1a). So, Eq. (7b) in the augmented formulation now reads

$$-\nabla \cdot (\varepsilon \mathbf{u}) - \ell^2 \nabla \cdot (\varepsilon \nabla p) = g + \ell^2 \nabla \cdot \mathbf{f}$$

and Eq. (19b) is now

$$b_h(q_h, \mathbf{u}_h) + s_h(p_h, q_h) = (g + \ell^2 \nabla \cdot \mathbf{f}, q_h).$$

Let us remind that in this case, the consistency terms that have been eliminated from (18) must be kept now. This straightforward generalization of our approach makes it suitable for the approximation of the so-called generalized formulations of Maxwell’s equations, which is a key ingredient in the numerical simulation of plasmas via Vlasov–Maxwell approximations. Roughly speaking, these solutions are such that  $p \neq 0$ . Since  $\mathbf{f}$  is numerically obtained in some cases,  $\nabla \cdot \mathbf{f}$  is going to be close to zero at most. Formulations that essentially assume that  $p = 0$  in their definition are not appropriate for these problems. We refer to [12,6] and references therein for a detailed exposition of these concepts.

**Remark 3.3.** The interior penalty stabilization terms in (20) require a value of the physical parameters on the faces. In general, we could take the value of  $\lambda$  on the faces (similarly for  $\varepsilon$ ) as  $\{\lambda^p\}^{\frac{1}{p}}$ , for  $1 \leq p \leq \infty$ , e.g. the choice  $p = \infty$  was considered in [24], even though only constant coefficients were used in the numerical experiments. Anyway, in the worst case scenario, the largest difference between any choice of  $p$  is a factor 2. So, we absorb this in the algorithmic constants of the interior penalty terms, and consider  $p = 1$  only.

Let us make some comments about the resulting formulation for the limit cases of cG and dG-type approximation spaces. In the first case, we can easily see that all the interior face (edge) terms cancel out and we recover the original cG formulation in [4]. However, when considering the dG case, we do not recover the interior penalty formulation in [24]. Two additional terms appear, namely the element interior stabilization terms:

$$\frac{c_u}{\ell^2} \int_{\mathcal{T}_h} \frac{h_l^2}{\varepsilon} \nabla \cdot (\varepsilon \mathbf{u}_h) \nabla \cdot (\varepsilon \mathbf{v}_h) + \ell^2 \int_{S_h} \varepsilon \nabla p_h \cdot \nabla q_h.$$

These terms are required for stability purposes when the inclusions

$$\nabla \cdot V_h \subseteq Q_h, \quad \nabla Q_h \subseteq V_h \tag{21}$$

are not true. We can easily see that for dG equal order FE approximations these inclusions are satisfied; since the method in [24] was restricted to this particular case, these terms were not needed. However, in the most general case, in which we consider a dG formulation with different approximation order for  $V_h$  and  $Q_h$ , or we consider the combined cG–dG approach, these terms cannot be neglected.

Further, these new terms weaken the constraints over the algorithmic parameters  $(c_{tu}, c_{nu}, c_{np})$ . The choice for these values is  $(10k^2, 1, 1)$ ,  $k$  being the order of approximation of  $\mathbf{u}$ , as suggested in [24]; the dependence of  $c_{tu}$  with respect to  $k$  has been

chosen in order to satisfy the assumption that  $c_{tu} > C_{inv}$  holds. On the other hand, upper bounds are also needed for stability reasons too, since in the limit  $(c_{tu}, c_{nu}, c_{np}) \rightarrow (\infty, \infty, \infty)$ , the dG method tends to the cG one, which is unstable. When adding the interior element terms that allow to avoid the assumption over the inclusions (21), the formulation is well posed in this limit, and so, there are no theoretical upper bounds for these coefficients.<sup>1</sup> We refer to Section 4 for some numerical results in this direction.

In the following, we perform the numerical analysis of the cG–dG formulation. First, let us introduce some norms for the stability analysis of the method:

$$\begin{aligned} \|\mathbf{u}_h\|_h &:= \|\lambda^{\frac{1}{2}} \nabla \times \mathbf{u}_h\|_{S_h} + \|\{\lambda\}^{\frac{1}{2}} h_{\perp}^{-\frac{1}{2}} \llbracket \mathbf{u}_h \rrbracket_t\|_{\mathcal{F}_h} + \ell^{-1} \|\varepsilon^{-\frac{1}{2}} h_t \nabla \cdot (\varepsilon \mathbf{u}_h)\|_{S_h} + \ell^{-1} \|h_{\perp}^{\frac{1}{2}} \{\varepsilon\}^{-\frac{1}{2}} \llbracket \varepsilon \mathbf{u}_h \rrbracket\|_{\mathcal{F}_h}, \\ \|\mathbf{p}_h\|_h &:= \ell \|\varepsilon^{\frac{1}{2}} \nabla p_h\|_{S_h} + \ell \|h_{\perp}^{-\frac{1}{2}} \{\varepsilon\}^{\frac{1}{2}} \llbracket p_h \rrbracket\|_{\mathcal{F}_h}. \end{aligned} \tag{22}$$

The norm in the product space  $V_h \times Q_h$  is denoted by  $\|\|\mathbf{u}_h, p_h\|\|_h := \|\mathbf{u}_h\|_h + \|p_h\|_h$ , whereas the norm that also includes  $L^2$  stability over  $\mathbf{u}_h$  is simply denoted by  $\|\|\mathbf{u}_h, p_h\|\| := \|\|\mathbf{u}_h, p_h\|\|_h + \ell^{-1} \|\varepsilon^{\frac{1}{2}} \mathbf{u}_h\|$ . Let us denote the bilinear form of the problem as

$$c_h(\mathbf{u}_h, p_h, \mathbf{v}_h, q_h) := a_h(\mathbf{u}_h, \mathbf{v}_h) - b_h(p_h, v_h) + b_h(q_h, u_h) + s_h(p_h, q_h). \tag{23}$$

In the next theorem, we prove coercivity of this bilinear form with respect to  $\|\|\cdot\|\|$ . This analysis is inspired by the results in [4,24] for the cG and dG versions, respectively. For the sake of conciseness, we consider a quasi-uniform and regular family of finite element partitions, and so we can consider  $h_I = h_{\perp} = h$  in the following proofs. Anyway, these proofs apply to the general case, with minor modifications. In the next proofs, we will denote by  $C_{\lambda, \varepsilon}$  the constants that can depend on the physical parameters but not on  $h$ .

**Theorem 3.1.** *The stabilized bilinear form (23) with the expressions in (20), with  $c_{tu} > C_{inv}$ , satisfies the following coercivity property:*

$$\alpha_{\lambda, \varepsilon} \|\|\mathbf{u}_h, p_h\|\|^2 \leq c_h(\mathbf{u}_h, p_h, \mathbf{u}_h, p_h) + \|\varepsilon^{-\frac{1}{2}} \mathbf{g}\|^2, \quad (\mathbf{u}_h, p_h) \in V_h \times Q_h$$

for a constant  $\alpha_{\lambda, \varepsilon} > 0$  uniform with respect to  $h$  that depends on the physical parameters.

**Proof.** The stability of the problem in the mesh-dependent norm is straightforward. We easily obtain:

$$\begin{aligned} c_h(\mathbf{u}_h, p_h, \mathbf{u}_h, p_h) &= \|\lambda^{\frac{1}{2}} \nabla \times \mathbf{u}_h\|_{S_h}^2 + c_{tu} \|\{\lambda\}^{\frac{1}{2}} h_{\perp}^{-\frac{1}{2}} \llbracket \mathbf{u}_h \rrbracket_t\|_{\mathcal{F}_h}^2 + \frac{C_u}{\ell^2} \|\varepsilon^{-\frac{1}{2}} h \nabla \cdot \mathbf{u}_h\|_{S_h}^2 + \frac{C_{nu}}{\ell_{\lambda}^2} \|h^{\frac{1}{2}} \{\varepsilon\}^{-\frac{1}{2}} \llbracket \varepsilon \mathbf{u}_h \rrbracket\|_{\mathcal{F}_h}^2 + \ell^2 \|\varepsilon^{\frac{1}{2}} \nabla p_h\|_{S_h}^2 \\ &\quad + \ell^2 \|h^{-\frac{1}{2}} \{\varepsilon\}^{\frac{1}{2}} \llbracket p_h \rrbracket\|_{\mathcal{F}_h}^2 - 2 \int_{\mathcal{F}_h} \llbracket \mathbf{u}_h \rrbracket_t \cdot \{\nabla \times \mathbf{u}_h\}. \end{aligned}$$

Now, using the lifting operator  $\mathcal{L}$  defined in [27, Section 5.1],

$$\int_{\Omega} \mathcal{L}(\mathbf{v}) \cdot \lambda \mathbf{w}_h := \int_{\mathcal{F}_h} \mathbf{v} \cdot \{\lambda \mathbf{w}_h\}, \quad \forall \mathbf{w}_h \in D_h,$$

where  $D_h$  is a space of possibly discontinuous piecewise polynomials such that  $\nabla \times V_h \subset D_h$ , and the continuity property

$$\|\lambda^{\frac{1}{2}} \mathcal{L}(\llbracket \mathbf{v}_h \rrbracket_t)\| \leq C_{inv} h^{-\frac{1}{2}} \|\lambda^{\frac{1}{2}} \llbracket \mathbf{v}_h \rrbracket_t\|_{\mathcal{F}_h}$$

proved in [27], and using that  $\lambda$  is piecewise constant on patches, we get

$$\begin{aligned} \int_{\mathcal{F}_h} \llbracket \mathbf{u}_h \rrbracket_t \{\lambda \nabla \times \mathbf{u}_h\} &= \int_{\Omega} \mathcal{L}(\llbracket \mathbf{u}_h \rrbracket_t) \cdot \lambda \nabla \times \mathbf{u}_h \\ &\leq C_{inv} h^{-\frac{1}{2}} \|\{\lambda\}^{\frac{1}{2}} \llbracket \mathbf{u}_h \rrbracket_t\|_{\mathcal{F}_h} \|\lambda^{\frac{1}{2}} \nabla \times \mathbf{u}_h\| \leq \frac{C_{inv}^2}{2\delta} \|\lambda^{\frac{1}{2}} \nabla \times \mathbf{u}_h\|^2 + \frac{\delta h^{-1}}{2} \|\{\lambda\}^{\frac{1}{2}} \llbracket \mathbf{u}_h \rrbracket_t\|_{\mathcal{F}_h}^2. \end{aligned} \tag{24}$$

Using the fact that  $C_{inv} < c_{tu}$ , we take  $C_{inv}^2 < \delta < c_{tu}^2$ . This way, we can absorb all these terms by  $\|\|\mathbf{u}_h, p_h\|\|_h^2$ . At this point, it only remains to prove that  $\ell^{-1} \|\varepsilon^{\frac{1}{2}} \mathbf{u}_h\| \leq \|\|\mathbf{u}_h, p_h\|\|_h$ . Let us consider the auxiliary problem:

$$\nabla \times \lambda \nabla \times \mathbf{z} + \varepsilon \nabla \varphi = \varepsilon \mathbf{u}_h, \quad \nabla \cdot (\varepsilon \mathbf{z}) = 0, \tag{25}$$

with  $\mathbf{n} \times \mathbf{z} = 0$  and  $\varphi = 0$  on  $\partial\Omega$ . By the stability of the continuous problem we have:

$$\ell^{-1} \|\lambda^{\frac{1}{2}} \nabla \times \mathbf{z}\| + \|\varepsilon^{\frac{1}{2}} \nabla \varphi\| \leq \|\varepsilon^{\frac{1}{2}} \mathbf{u}_h\|.$$

Given  $\mathbf{w} := \lambda^{\frac{1}{2}} \nabla \times \mathbf{z}$ , we know from [21] that there exists  $\mathbf{w}_0 \in H_0^1(\Omega)$  such that

$$\nabla \times \mathbf{w}_0 = \nabla \times \mathbf{w}, \quad \|\mathbf{w}_0\|_1 \lesssim \|\mathbf{w}\|_{H_0(\text{curl}, \Omega)} \leq C_{\lambda, \varepsilon} \|\varepsilon^{\frac{1}{2}} \mathbf{u}_h\|.$$

<sup>1</sup> In any case, super-penalty formulations would negatively affect the performance of linear solvers.

Now, we multiply the first equation in the auxiliary problem by  $\mathbf{u}_h$  and integrate over  $\Omega$ , getting

$$\int_{\Omega} \mathbf{u}_h \cdot \nabla \times \lambda \nabla \times \mathbf{z} + \int_{\Omega} \mathbf{u}_h \cdot \varepsilon \nabla \varphi = \|\varepsilon^{\frac{1}{2}} \mathbf{u}_h\|^2. \tag{26}$$

The first term is integrated by parts, obtaining

$$\begin{aligned} \int_{\Omega} \mathbf{u}_h \cdot \nabla \times \lambda \nabla \times \mathbf{z} &= \int_{S_h} \lambda^{\frac{1}{2}} \nabla \times \mathbf{u}_h \cdot \mathbf{w}_0 - \int_{\mathcal{F}_h} \llbracket \lambda^{\frac{1}{2}} \mathbf{u}_h \rrbracket_t \cdot \{\mathbf{w}_0\} - \int_{\mathcal{F}_h} \mathbf{n} \times \left\{ \lambda^{\frac{1}{2}} \mathbf{u}_h \right\} \cdot \mathbf{w}_0 \\ &\leq C_{\lambda, \varepsilon} \left( \|\lambda^{\frac{1}{2}} \nabla \times \mathbf{u}_h\|_{S_h} \ell \|\mathbf{w}_0\|_1 + \|h^{\frac{1}{2}} \mathbf{w}_0\|_{\mathcal{F}_h} \left\{ \lambda^{\frac{1}{2}} \right\} h^{-\frac{1}{2}} \|\llbracket \mathbf{u}_h \rrbracket_t\|_{\mathcal{F}_h} \right) \leq C_{\lambda, \varepsilon} (\|\mathbf{u}_h, p_h\|_h \ell \|\mathbf{w}_0\|_1), \end{aligned} \tag{27}$$

where we have used (12). For the second term, let us introduce  $\varphi_h$ , an optimal projection of  $\varphi$  onto  $Q_h$  with  $H^1$ -continuity that keeps the homogeneous boundary condition, e.g. the Scott-Zhang projector (see [8]). We get

$$\int_{\Omega} \mathbf{u}_h \cdot \varepsilon \nabla \varphi = \int_{\Omega} \mathbf{u}_h \cdot \varepsilon \nabla (\varphi - \varphi_h) - \ell^2 \int_{S_h} \varepsilon \nabla \varphi_h \cdot \nabla p_h + (\mathbf{g}, \varphi_h), \tag{28}$$

where we have used the divergence constraint discrete equation. Now, we treat the first term as follows:

$$\begin{aligned} \int_{\Omega} \mathbf{u}_h \cdot \varepsilon \nabla (\varphi - \varphi_h) &= - \int_{\Omega} \nabla \cdot (\varepsilon \mathbf{u}_h) (\varphi - \varphi_h) + \int_{\mathcal{F}_h} \llbracket \varepsilon \mathbf{u}_h \rrbracket (\varphi - \varphi_h) \\ &\leq C_{\lambda, \varepsilon} \left( h \ell^{-1} \|\varepsilon^{\frac{1}{2}} \nabla \cdot \mathbf{u}_h\|_{S_h} + h^{\frac{1}{2}} \ell^{-1} \|\llbracket \varepsilon^{\frac{1}{2}} \mathbf{u}_h \rrbracket\| \right) \left( h^{-1} \ell \|\varepsilon^{\frac{1}{2}} (\varphi - \varphi_h)\| + h^{-\frac{1}{2}} \ell \|\varepsilon^{\frac{1}{2}} (\varphi - \varphi_h)\|_{\mathcal{F}_h} \right) \\ &\leq C_{\lambda, \varepsilon} \left( h \ell^{-1} \|\varepsilon^{\frac{1}{2}} \nabla \cdot \mathbf{u}_h\|_{S_h} + h^{\frac{1}{2}} \ell^{-1} \|\varepsilon^{\frac{1}{2}} \llbracket \mathbf{u}_h \rrbracket\| \right) \ell \|\varphi\|_1 \end{aligned} \tag{29}$$

The treatment of the last terms is easy:

$$-\ell^2 \int_{S_h} \varepsilon \nabla \varphi \cdot \nabla p_h + (\mathbf{g}, \varphi_h) \leq \left( \ell \|\varepsilon^{\frac{1}{2}} \nabla p_h\|_{S_h} + \ell^{-1} \|\varepsilon^{-\frac{1}{2}} \mathbf{g}\| \right) \ell \|\varepsilon^{\frac{1}{2}} \nabla \varphi\|.$$

Combining all these results, we can show that  $\ell^{-1} \|\varepsilon^{\frac{1}{2}} \mathbf{u}_h\| \leq C_{\lambda, \varepsilon} \|\mathbf{u}_h, p_h\|_h + \ell^{-1} \|\varepsilon^{-\frac{1}{2}} \mathbf{g}_h\|$ . This proves the theorem.  $\square$

The next result states optimal convergence for the combined cG–dG formulation. We define the norms,

$$e_1(\mathbf{v}, q) := \|\mathbf{v}, q\| + \frac{h^{\frac{1}{2}}}{\ell} \|\{\varepsilon\}^{\frac{1}{2}} \mathbf{v}\|_{\mathcal{F}_h}, \quad e_2(\mathbf{v}) := \|\lambda^{\frac{1}{2}} \mathbf{v}\| + h^{\frac{1}{2}} \|\{\lambda\}^{\frac{1}{2}} \mathbf{v}\|_{\mathcal{F}_h}. \tag{30}$$

as well as the error function:

$$E_h(\mathbf{v}, q) := \inf_{\mathbf{v}_h \in V_h, q_h \in Q_h} e_1(\mathbf{v} - \mathbf{v}_h, q - q_h) + \inf_{\mathbf{w}_h \in V_h} e_2(\nabla \times \mathbf{v} - \mathbf{w}_h).$$

**Theorem 3.2.** *The solution  $(\mathbf{u}_h, p_h) \in V_h \times Q_h$  of system (19)–(20) with  $c_{tu} \geq C_{inv}$  satisfies the error estimate*

$$\|\mathbf{u}_h - \mathbf{u}, p_h - p\| \leq C_{\lambda, \varepsilon} E_h(\mathbf{u}, p).$$

where  $(\mathbf{u}, p)$  is the solution of the continuous problem.

**Proof.** Since there is no consistency error, we can easily check that for any  $\tilde{\mathbf{u}}_h \in V_h$  and  $\tilde{p}_h \in Q_h$ , we have

$$c_h(\tilde{\mathbf{u}}_h - \mathbf{u}_h, \tilde{p}_h - p_h, \tilde{\mathbf{u}}_h - \mathbf{u}_h, \tilde{p}_h - p_h) = c_h(\tilde{\mathbf{u}}_h - \mathbf{u}, \tilde{p}_h - p, \tilde{\mathbf{u}}_h - \mathbf{u}_h, \tilde{p}_h - p_h).$$

Stability has already been proved above. The only remaining point is to bound the interpolation error. Let us prove that

$$c_h(\tilde{\mathbf{u}}_h - \mathbf{u}, \tilde{p}_h - p, \mathbf{v}_h, q_h) \lesssim (e_1(\mathbf{u} - \tilde{\mathbf{u}}_h, p - \tilde{p}_h) + e_2(\nabla \times \mathbf{u} - \mathbf{w}_h)) \|\tilde{\mathbf{v}}_h, q_h\| \tag{31}$$

for any  $\mathbf{v}_h, \mathbf{w}_h \in V_h$  and  $q_h \in Q_h$ . The bound for the symmetric jump terms is straightforward. For the sake of conciseness, we only bound the most interesting terms. The element interior stabilization term for the divergence is treated as follows:

$$\begin{aligned} h^2 \int_{S_h} \varepsilon^{-1} \nabla \cdot (\varepsilon \tilde{\mathbf{u}}_h - \varepsilon \mathbf{u}) \nabla \cdot (\varepsilon \mathbf{v}_h) &= -h^2 \sum_{S \in S_h} \int_{S_h} \varepsilon^{-1} (\tilde{\mathbf{u}}_h - \mathbf{u}) \nabla \nabla \cdot (\varepsilon \mathbf{v}_h) + h^2 \sum_{S \in S_h} \int_{\partial S} \varepsilon^{-1} \mathbf{n} \cdot (\tilde{\mathbf{u}}_h - \mathbf{u}) \nabla \cdot (\varepsilon \mathbf{v}_h) \\ &\lesssim \sum_{S \in S_h} \left( \|\varepsilon^{\frac{1}{2}} (\tilde{\mathbf{u}}_h - \mathbf{u})\|_S h \|\varepsilon^{-\frac{1}{2}} \nabla \cdot (\varepsilon \mathbf{v}_h)\|_S + h^{\frac{1}{2}} \|\varepsilon^{\frac{1}{2}} (\tilde{\mathbf{u}}_h - \mathbf{u})\|_{\partial S} h^{\frac{3}{2}} \|\varepsilon^{-\frac{1}{2}} \nabla \cdot (\varepsilon \mathbf{v}_h)\|_{\partial S} \right) \\ &\lesssim \left( \|\varepsilon^{\frac{1}{2}} (\tilde{\mathbf{u}}_h - \mathbf{u})\| + h^{\frac{1}{2}} \|\{\varepsilon\}^{\frac{1}{2}} (\tilde{\mathbf{u}}_h - \mathbf{u})\|_{\mathcal{F}_h} \right) h \|\varepsilon^{-\frac{1}{2}} \nabla \cdot (\varepsilon \mathbf{v}_h)\|, \end{aligned}$$

where we have used integration-by-parts and inverse inequalities. For any  $\mathbf{w}_h \in V_h$ , we also have:

$$\begin{aligned} \int_{\mathcal{F}_h} \llbracket \mathbf{v}_h \rrbracket_t \cdot \{ \lambda \nabla \times (\tilde{\mathbf{u}}_h - \mathbf{u}) \} &= \int_{\mathcal{F}_h} \llbracket \mathbf{v}_h \rrbracket_t \cdot \{ \lambda \nabla \times \tilde{\mathbf{u}}_h - \lambda \mathbf{w}_h \} + \int_{\mathcal{F}_h} \llbracket \mathbf{v}_h \rrbracket_t \cdot \{ \lambda \mathbf{w}_h - \lambda \nabla \times \mathbf{u} \} \\ &\lesssim h^{-\frac{1}{2}} \|\{ \lambda \}^{\frac{1}{2}} \llbracket \mathbf{v}_h \rrbracket_t\|_{\mathcal{F}_h} \left( \|\lambda^{\frac{1}{2}} \nabla \times (\tilde{\mathbf{u}}_h - \mathbf{u})\| + \|\lambda^{\frac{1}{2}} (\mathbf{w}_h - \nabla \times \mathbf{u})\| + h^{\frac{1}{2}} \|\{ \lambda \}^{\frac{1}{2}} (\mathbf{w}_h - \nabla \times \mathbf{u})\|_{\mathcal{F}_h} \right). \end{aligned}$$

where we have used again inverse inequalities. The rest of terms are easily bounded. Finally, using the coercivity of  $c_h$  proved in Theorem 3.1 in expression (31), together with the fact that  $\|\mathbf{u} - \mathbf{v}_h\| \lesssim e_1(\mathbf{u} - \mathbf{v}_h)$  for any  $\mathbf{v}_h \in V_h$  and the triangle inequality, we prove the theorem.  $\square$

For smooth solutions, i.e.  $\mathbf{u} \in H^1(\Omega)$ , the previous error bounds are optimal. The case of singular solutions is not so straightforward. Under some assumptions over the typology of the mesh, we can prove that  $\lim_{h \rightarrow 0} E_h(\mathbf{u}, p) = 0$  without regularity requirements (see [4] and references therein). In particular, for two-dimensional problems, two types of macro-element meshes have been found to be suitable, namely, the so called crossed-box and Powell–Sabin meshes (see Fig. 1).

Let us remark the fact that the need to use macro-element meshes comes from approximability arguments for singular solutions instead of stability reasons. Similar constraints have been found in [17,10]. One can show, for the constant coefficients case, that at least  $\mathbf{u} \in H^s(\Omega)$  with  $s > \frac{1}{2}$ , and  $\nabla \times \mathbf{u} \in H^s(\Omega)$  (see [16] for a detailed exposition). So, the second component of the error function, that measures the distance between  $\nabla \times \mathbf{u}$  and  $V_h$  measured in terms of  $e_2$ , cannot spoil the convergence towards singular solutions.

### 3.2. An alternative formulation based on projections

As commented above, the previous cG–dG algorithm is not reduced to the dG interior penalty formulation in [24]. We can however consider a modified formulation, in which the element interior stabilization is reduced. The idea consists of stabilizing only the components of  $\nabla \cdot \mathbf{u}_h$  and  $\nabla p_h$  that are orthogonal to  $Q_h$  and  $V_h$ , respectively; the corresponding FE projections are bounded by the Galerkin terms. Therefore, the new method consists of (19) with the following new expressions for the bilinear forms:

$$\begin{aligned} a_h(\mathbf{u}_h, \mathbf{v}_h) &:= \int_{S_h} \lambda \nabla \times \mathbf{v}_h \cdot \nabla \times \mathbf{u}_h - \int_{\mathcal{F}_h} \llbracket \mathbf{v}_h \rrbracket_t \cdot \{ \lambda \nabla \times \mathbf{u}_h \} - \int_{\mathcal{F}_h} \llbracket \mathbf{u}_h \rrbracket_t \cdot \{ \lambda \nabla \times \mathbf{v}_h \} \\ &\quad + c_{tu} \int_{\mathcal{F}_h} \frac{\{ \lambda \}}{h_{\perp}} \llbracket \mathbf{u}_h \rrbracket_t \cdot \llbracket \mathbf{v}_h \rrbracket_t + \frac{c_u}{\ell^2} \int_{\mathcal{T}_h} \frac{h_l^2}{\varepsilon} P_{Q_h}^{\perp} (\nabla \cdot (\varepsilon \mathbf{u}_h)) \nabla \cdot (\varepsilon \mathbf{v}_h) + \frac{c_{nu}}{\ell^2} \int_{\mathcal{F}_h} \frac{h_{\perp}}{\{ \varepsilon \}} \llbracket \varepsilon \mathbf{u}_h \rrbracket \llbracket \varepsilon \mathbf{v}_h \rrbracket, \tag{32} \\ s_h(p_h, q_h) &:= \ell^2 \int_{S_h} \varepsilon P_{V_h}^{\perp} (\nabla p_h) \cdot \nabla q_h + c_{np} \ell^2 \int_{\mathcal{F}_h} \frac{\{ \varepsilon \}}{h_{\perp}} \llbracket p_h \rrbracket \cdot \llbracket q_h \rrbracket, \end{aligned}$$

where  $P_{Q_h}$  and  $P_{V_h}$  are the  $L^2$  projections onto  $Q_h$  and  $V_h$ , respectively. These projections can be defined for each patch of  $S_h$ , where  $\lambda$  and  $\varepsilon$  are considered constant. The introduction of the orthogonal projection in the divergence term does not introduce any problem in the stability and convergence analysis of the method. However, the orthogonal projection in the gradient term introduces some complications in the following analysis. It motivates the introduction of a norm weaker than  $\|\cdot\|$ , in which we prove stability and convergence of the method:

$$\|\|\mathbf{u}_h, p_h\|\|_w := \|\mathbf{u}_h\|_h + \ell^{-1} \|\varepsilon^{\frac{1}{2}} \mathbf{u}_h\| + h \|\varepsilon^{\frac{1}{2}} P_{V_h} (\nabla p_h)\|_{S_h} + \ell \|\varepsilon^{\frac{1}{2}} P_{V_h}^{\perp} (\nabla p_h)\|_{S_h} + \ell \|h^{-\frac{1}{2}} \{ \varepsilon \}^{\frac{1}{2}} \llbracket p_h \rrbracket\|_{\mathcal{F}_h}.$$

In any case, the method exhibits good stability and convergence behavior even for the approximation of singular solutions (see Section 4). Stability is proved in the next theorem; we remark the fact that in this case stability is stated in terms of an inf–sup condition, instead of coercivity, as in the orthogonal subgrid scale stabilization (OSS) method analyzed in [14].

**Theorem 3.3.** *The bilinear form (23) with the expressions in (32) and  $c_{tu} > C_{inv}$  satisfies the inf–sup condition*

$$\inf_{(\mathbf{u}_h, p_h) \in V_h \times Q_h} \sup_{(\mathbf{v}_h, q_h) \in V_h \times Q_h} \frac{c_h(\mathbf{u}_h, p_h, \mathbf{v}_h, q_h)}{\|\|\mathbf{u}_h, p_h\|\|_w \|\|\mathbf{v}_h, q_h\|\|_w} \geq \beta_{\lambda, \varepsilon},$$

for a constant  $\beta_{\lambda, \varepsilon} > 0$  uniform with respect to  $h$  that depends on the physical parameters.

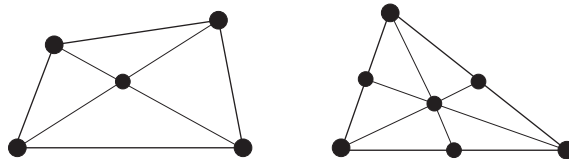


Fig. 1. Crossed-box (left) and Powell–Sabin (right) macro-element typologies in 2D.

**Proof.** To concentrate only on the difficulties introduced by  $P_{Q_h}$  and  $P_{V_h}$ , assume for simplicity that  $\lambda = 1$ ,  $\varepsilon = 1$  and  $\ell = 1$ . As above, we initially test the system against  $(\mathbf{u}_h, p_h)$ . Analogously to Theorem 3.1, we are able to prove stability for all the terms in  $\|\cdot\|_w$  but those associated to the projections  $hP_{Q_h}(\nabla \cdot \mathbf{u}_h)$  and  $hP_{V_h}(\nabla p_h)$ . Stability over the first term is obtained taking  $(\mathbf{0}, \delta h^2 P_{Q_h}(\nabla \cdot \mathbf{u}_h))$  as test functions in (19)–(32), where  $\delta > 0$  is an appropriate constant to be defined. We obtain:

$$c_h(\mathbf{u}_h, p_h, \mathbf{0}, \delta h^2 P_{Q_h}(\nabla \cdot \mathbf{u}_h)) = \delta h^2 \|P_{Q_h}(\nabla \cdot \mathbf{u}_h)\|^2 - \delta h^2 \int_{\mathcal{F}_h^0} \{P_{Q_h}(\nabla \cdot \mathbf{u}_h)\} \llbracket \mathbf{u}_h \rrbracket + \delta h^2 \int_{\mathcal{S}_h} \nabla P_{Q_h}(\nabla \cdot \mathbf{u}_h) \cdot \nabla p_h + \delta h \int_{\mathcal{F}_h} \llbracket p_h \rrbracket \cdot \llbracket P_{Q_h}(\nabla \cdot \mathbf{u}_h) \rrbracket.$$

Using inverse inequalities (10)–(12), we easily obtain the bound:

$$c_h(\mathbf{u}_h, p_h, \mathbf{0}, \delta h^2 P_{Q_h}(\nabla \cdot \mathbf{u}_h)) \geq \frac{\delta h^2}{4} \|P_{Q_h}(\nabla \cdot \mathbf{u}_h)\|^2 - \delta c_1 h \|\llbracket \mathbf{u}_h \rrbracket\|_{\mathcal{F}_h^0}^2 - \delta c_2 \|\nabla p_h\|_{\mathcal{S}_h}^2 - \delta c_3 h^{-1} \|\llbracket p_h \rrbracket\|_{\mathcal{F}_h}^2,$$

for appropriate constants  $c_1, c_2$  and  $c_3$ . On the other hand, testing system (19)–(32) against the function  $(\varphi h^2 P_{V_h}(\nabla p_h), 0)$ , with  $\varphi > 0$  to be defined, we get:

$$\begin{aligned} c_h(\mathbf{u}_h, p_h, \varphi h^2 P_{V_h}(\nabla p_h), 0) &= \varphi h^2 \|P_{V_h}(\nabla p_h)\|^2 + \varphi h^2 \int_{\mathcal{S}_h} \nabla \times P_{V_h}(\nabla p_h) \cdot \nabla \times \mathbf{u}_h - \varphi h^2 \int_{\mathcal{F}_h} \llbracket P_{V_h}(\nabla p_h) \rrbracket_t \cdot \{\nabla \times \mathbf{u}_h\} \\ &\quad - \varphi h^2 \int_{\mathcal{F}_h} \llbracket \mathbf{u}_h \rrbracket_t \cdot \{\nabla \times P_{V_h}(\nabla p_h)\} + \varphi h c_{tu} \int_{\mathcal{F}_h} \llbracket \mathbf{u}_h \rrbracket_t \cdot \llbracket P_{V_h}(\nabla p_h) \rrbracket_t + \varphi h^4 c_u \int_{\mathcal{S}_h} P_{Q_h}^\perp(\nabla \\ &\quad \cdot \mathbf{u}_h) \nabla \cdot P_{V_h}(\nabla p_h) + \varphi h^3 c_{nu} \int_{\mathcal{F}_h^0} \llbracket \mathbf{u}_h \rrbracket \llbracket P_{V_h}(\nabla p_h) \rrbracket - \varphi h^2 \int_{\mathcal{F}_h} \llbracket p_h \rrbracket \cdot \{P_{V_h}(\nabla p_h)\}. \end{aligned} \tag{33}$$

The conflictive terms that do not allow full control over  $P_{V_h}(\nabla p_h)$  are those related to the curl-curl term, i.e. the second to fourth terms in the right-hand side of (33). After some manipulation, using expressions (10)–(12) properly, we obtain:

$$\begin{aligned} c_h(\mathbf{u}_h, p_h, \varphi h^2 P_{V_h}(\nabla p_h), 0) &= \frac{\varphi h^2}{8} \|P_{V_h}(\nabla p_h)\|^2 - \varphi c_4 \|\nabla \times \mathbf{u}_h\|_{\mathcal{S}_h}^2 - \varphi c_5 h^{-1} \|\llbracket \mathbf{u}_h \rrbracket_t\|_{\mathcal{F}_h}^2 - \varphi c_6 h^4 \|P_{Q_h}^\perp(\nabla \cdot \mathbf{u}_h)\|_{\mathcal{S}_h}^2 \\ &\quad - \varphi c_7 h^3 \|\llbracket \mathbf{u}_h \rrbracket\|_{\mathcal{F}_h}^2 - \varphi c_8 h \|\llbracket p_h \rrbracket\|_{\mathcal{F}_h}^2. \end{aligned} \tag{34}$$

for appropriate constants  $c_4, \dots, c_8$ . Combining the previous results with  $\delta$  and  $\varphi$  small enough, we get

$$c_h(\mathbf{u}_h, p_h, \mathbf{u}_h + \varphi h^2 P_{V_h}(\nabla p_h), p_h + \delta h^2 P_{Q_h}(\nabla \cdot \mathbf{u}_h)) \gtrsim \|\mathbf{u}_h, p_h\|_w^2.$$

The remaining point is to prove that  $\|\varphi h^2 P_{V_h}(\nabla p_h), \delta h^2 P_{Q_h}(\nabla \cdot \mathbf{u}_h)\|_w \lesssim \|\mathbf{u}_h, p_h\|_w$ , which can be easily checked by using repeatedly (10) and (12).  $\square$

Again, the introduction of the orthogonal projection in the stabilization term for  $\nabla p_h$  introduces some complications in the convergence analysis, due to the weaker stability results. In particular, instead of bounding the error of the numerical solution by the one of the best FE approximation with respect to  $E_h(\cdot)$ , we are only able to bound the error related to  $\mathbf{u}$  by the one of the  $L^2$ -projector. In any case, this projector has optimal interpolation properties for smooth solutions (see, e.g. [8]).

**Theorem 3.4.** *The numerical solution  $(\mathbf{u}_h, p_h)$  of system (19)–(32) satisfies*

$$\|\mathbf{u}_h - \mathbf{u}, p_h - p\| \lesssim \inf_{q_h \in Q_h} e_1(\mathbf{u} - P_{V_h}(\mathbf{u}), p - q_h) + \inf_{\mathbf{w}_h \in V_h} e_2(\nabla \times \mathbf{u} - \mathbf{w}_h).$$

where  $(\mathbf{u}, p)$  is the solution of the continuous problem (2).

**Proof.** The term that complicates the analysis and forces to consider the  $L^2$  projector in the definition of the interpolation error is the following:

$$\int_{\Omega} \nabla q_h \cdot (P_{V_h}(\mathbf{u}) - \mathbf{u}) = \int_{\Omega} P_{V_h}^\perp(\nabla q_h) \cdot (P_{V_h}(\mathbf{u}) - \mathbf{u}) \lesssim \|P_{V_h}^\perp(\nabla q_h)\| \|P_{V_h}(\mathbf{u}_h) - \mathbf{u}\|.$$

We omit the rest of terms, since their bounds are obtained as in the proof of Theorem 3.2. Combining again stability and the bound for the interpolation error, we prove the theorem.  $\square$

**Remark 3.4.** Let us remark that an intermediate problem, in which the projection is only introduced in the divergence term, exhibits the stability result in Theorem 3.1 with respect to the strong norm  $\|\cdot\|$ , and the same happens for the convergence result in Theorem 3.2. We omit the details here, since it is straightforward from the previous analysis. As a conclusion, the fact that complicates the problem is the introduction of the projection on  $\nabla p_h$  in the term

$$\ell^2 \int_{S_h} \varepsilon \mathbf{P}_{V_h}^\perp(\nabla p_h) \cdot \nabla q_h.$$

This can hardly be motivated using the augmented formulation, but is perfectly acceptable interpreting this term as an additional stabilization term.

**Remark 3.5.** Consider the pure dG method and suppose that inclusions (21) hold, i.e. equal discontinuous interpolation for  $\mathbf{u}$  and  $p$  is used. Then  $P_{Q_h}^\perp(\nabla \cdot (\varepsilon \mathbf{v}_h)) = 0$  for any  $\mathbf{v}_h \in V_h$  and  $P_{V_h}^\perp(\nabla q_h) = 0$  for any  $q_h \in Q_h$ . The method (19) with the bilinear forms  $a_h$  and  $s_h$  given in (32) and  $b_h$  given in (20) reduces to the method proposed in [24].

## 4. Numerical experiments

### 4.1. The singular problem

In this section, we want to check how the previous approach is suitable for the numerical approximation of singular solutions of system (1). With this aim, we consider the datum  $\mathbf{f}$  such that the solution in polar coordinates  $(r, \theta)$  is:

$$\mathbf{u} = \nabla \left( r^{\frac{2n}{3}} \sin \frac{2n\theta}{3} \right) \quad (35)$$

in the nonconvex domain  $\Omega \equiv [-1, 1]^2 \setminus ([0, 1] \times [0, -1])$ , with one re-entrant corner. We have that  $\mathbf{u} \in H^{\frac{2n}{3}-\epsilon}(\Omega)$ , for any  $\epsilon > 0$ . We consider  $\lambda = \epsilon = 1$ . For  $n = 1$  we have a singular solution since  $\mathbf{u} \notin H^1(\Omega)^2$ . Larger values of  $n$  lead to smooth solutions.

In the following, we have considered all the algorithmic constants equal to one, except  $c_{\text{tu}} = 10$ , in order to satisfy  $c_{\text{tu}} > C_{\text{inv}}$  (see [24]).

### 4.2. The cG method

It has been proved in [4] that the nodal cG formulation (13) converges to the good solution even in the singular case. In order to show the behavior of the cG formulation, we have plotted the two components of  $\mathbf{u}$  in Figs. 2, 3 for the exact solution (35) with  $n = 1$ , as well as the solution of the stabilized cG formulation in (19)–(20) for a structured uniform mesh of 4096 linear triangular elements with a crossed-box macro-element structure (see Fig. 1). We see that the numerical approximation is close to the appropriate singular solution. On the other hand, we have performed this test for the same cG formulation but switching off the divergence stabilization term  $s_h$  in (13a); it is clear from Figs. 2, 3 that this term is not only needed for technical purposes but also basic for the good behavior of the algorithm. We remark that this term is required in order to get control over  $\|\mathbf{u}_h\|$ . Finally, we include the results obtained for a stabilized method in the *wrong* functional setting  $H^1(\Omega)^d \times L^2(\Omega)$ . The functional setting is changed by replacing  $\ell$  by  $h_i$  and vice versa in (14) (see [5] and [4, Section 4.2]). As expected, this method is affected by the approximability property, tending to a spurious solution. The convergence rates of these methods for different values of  $n$  can be found in [4].

The formulation with orthogonal projections (19)–(32) has been tested for the cG FE approximation. We can easily check that the weaker stability and convergence results also apply for the cG particular case. We have performed the convergence analysis for  $n = 1, 2, 4$  and  $h = 2^{-i}$  for  $i = 3, 4, 5, 6$  (see Fig. 4). Despite the stability and convergence theoretical results are slightly weaker than those in the original formulation (19)–(20), the numerical results are almost identical to those for the original cG formulation, that can be found in [4]. The method approximates well both singular and smooth solutions.

Finally, let us show the effect of the macro-element mesh typology in the convergence of the method towards singular solutions. In Fig. 5(a) and (b) we show the results obtained for the singular corner problem, by using a structured triangular mesh without this requirement. It becomes evident that the solution does not resemble the shape of the exact solution, with a triangle mesh of 6144 elements. We plot in Fig. 5(c) a zoom of the  $y$  component of the solution around the corner for a very fine mesh of 393,216 elements. The solution still presents a weird shape that is not cured as the mesh is refined. Then, we plot in Fig. 6 the error for both the arbitrary and crossbox meshes. Out of these results, we conclude that the macro-element structure clearly reduces the numerical error and the convergence rates for linear approximations, more significantly with respect to  $\|\nabla \times (\mathbf{u} - \mathbf{u}_h)\|$ .

### 4.3. The dG method

Similar convergence results to those presented earlier can be found in [24] for the dG formulation. Since the first cG–dG formulation we propose in Section 3.1 includes additional terms in the dG limit, we aim at checking that these additional stabilization terms are harmless. In Fig. 7, we plot the numerical error for different norms using linear FEs, for both the original dG method and the *over-stabilized* one. We can easily check that the results are very similar for these two methods, even though the errors are always slightly smaller for the over-stabilized formulation. As a conclusion, the use of the cG–dG formulation (19)–(20) is suitable, and the fact that it involves additional stabilization terms that are not needed in the dG limit, when inclusions (21) are satisfied, does not represent any accuracy reduction. All these experiments agree with the theoretical results.

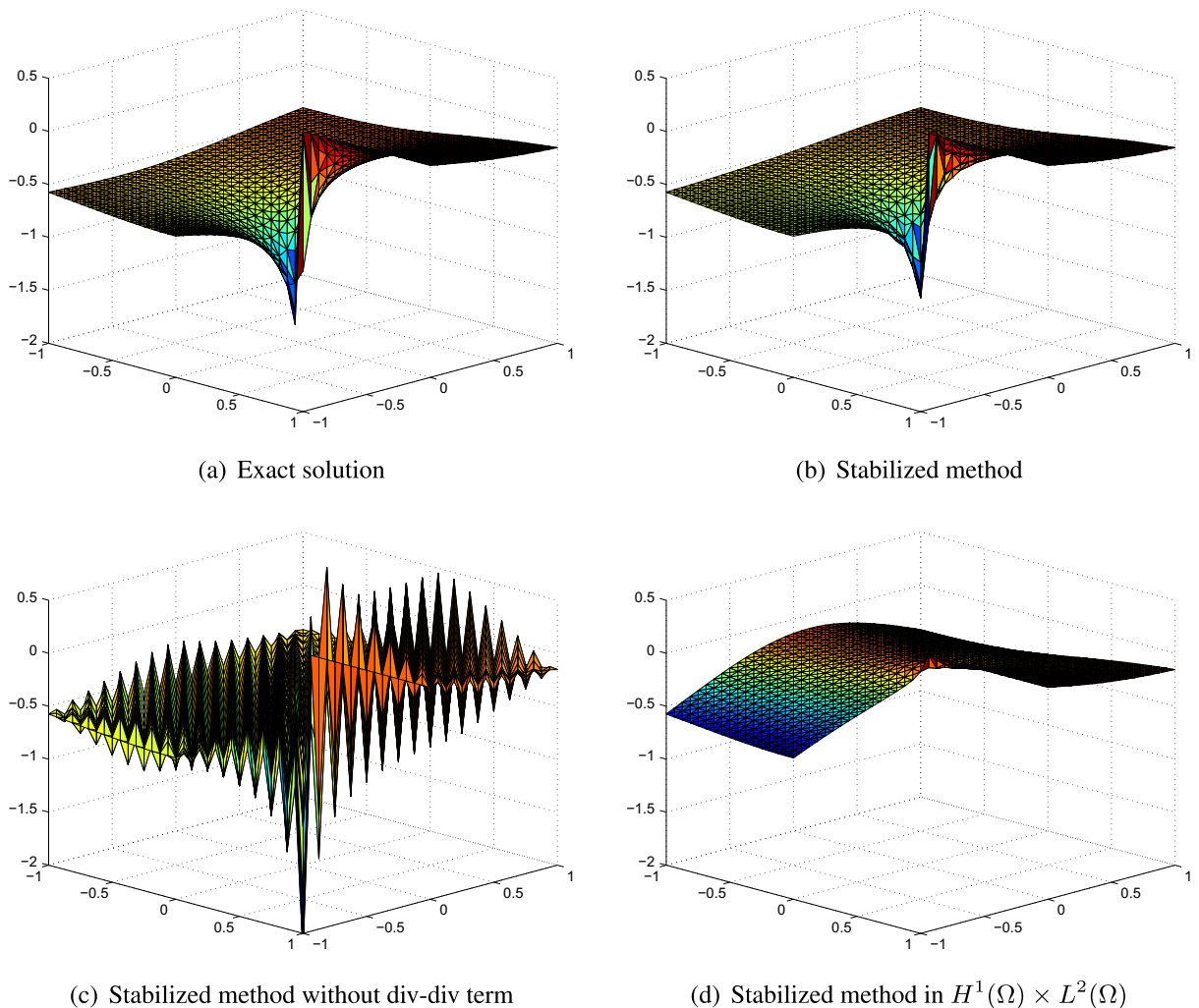


**Fig. 2.** Comparison of the exact and numerical solution for different approximations of the test problem with exact solution (35) for  $n = 1$ . Component  $u_x$ .

#### 4.4. The cG–dG method

Now, let us consider a simple cG–dG problem, in which we have split the domain into two different patches (see Fig. 8(a)). As defined above, the continuity between patches is weakly enforced via the interior penalty interface terms whereas the FE functions are continuous inside patches. In Fig. 8(b), we show how the error is reduced for the cG–dG formulation, for a refinement with characteristic mesh size  $2^{-i}$  with  $i = 3, 4, 5, 6$ . The convergence rates are excellent for the problem with singular solution.

Fig. 9 compares the error associated to the cG, dG and combined cG–dG formulation. In order to compare the different methods in terms of computational cost, we define an effective mesh size  $h_{\text{eff}} = L_0(n_{\text{dof}})^{-\frac{1}{d}}$ , where  $n_{\text{dof}}$  indicates the number of degrees of freedom.

We have considered both the error for  $\mathbf{u}$  in terms of the  $L^2$  norm and  $\|\cdot\|_h$  norm. From these results it is observed that the cG method is the best approach for this particular choice of the patches in terms of  $\|\mathbf{u} - \mathbf{u}_h\|$ . However, the cG–dG formulation is more accurate with respect to  $\|\mathbf{u} - \mathbf{u}_h\|_h$ . In any case, what becomes quite evident out of these results is the fact that a full dG formulation is less accurate for the singular re-entrant corner problem than a cG formulation for a fixed computational cost. It justifies the combined cG–dG approach in the paper. In applications with discontinuous jumps, in which cG alone is not suitable, a combined formulation allows us to weaken continuity in the interfaces between different materials keeping accuracy for a low computational cost of the nodal cG formulation.

#### 4.5. Discontinuous physical coefficients with the cG–dG method

We finally solve a problem with discontinuous coefficients, in order to show the ability of the proposed approach to handle discontinuous solutions doubling only the degrees of freedom at the interface between materials. Since discontinuous

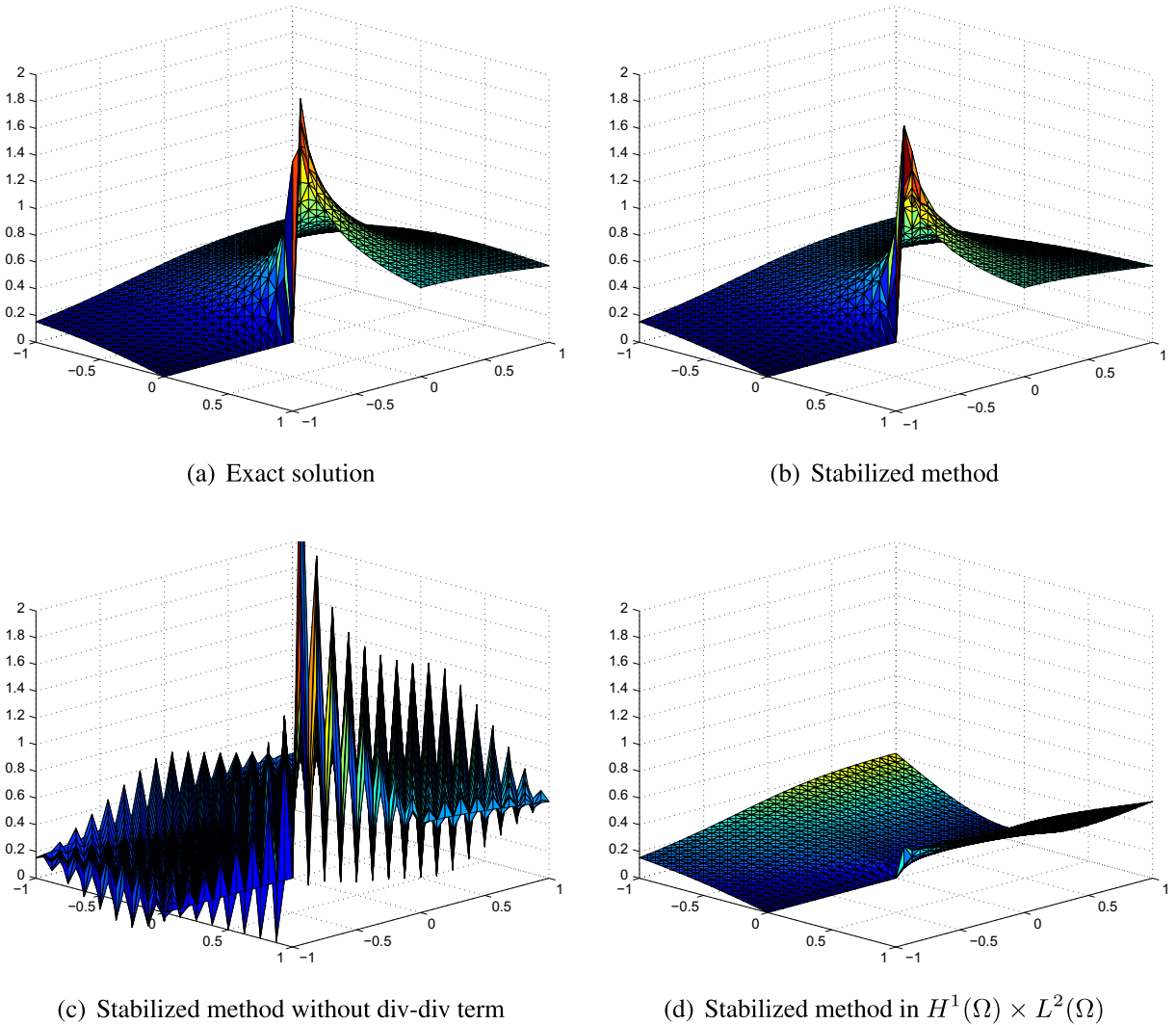


Fig. 3. Comparison of the exact and numerical solution for different approximations of the test problem with exact solution (35) for  $n = 1$ . Component  $u_y$ .

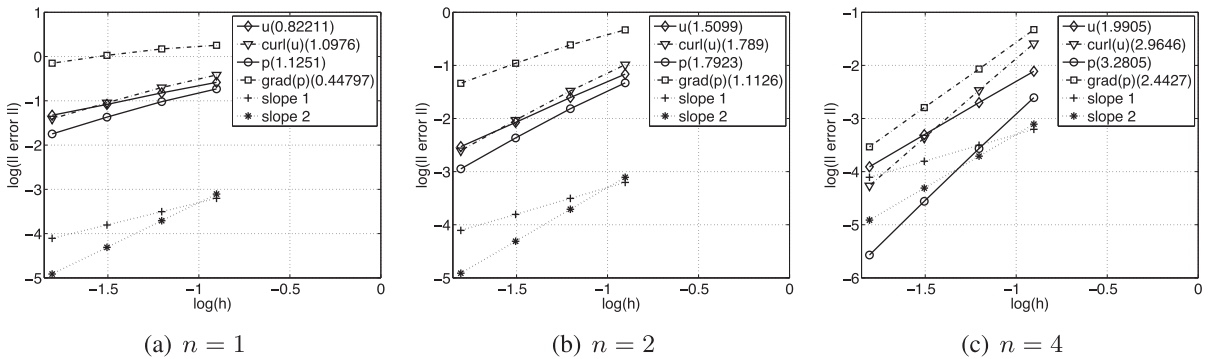


Fig. 4. Error plots for different quantities in  $L^2(\Omega)$  norm for Formulation (19)–(32) (with orthogonal projections) and the problem with analytical solution (35), for different values of  $n$ . Values in parenthesis indicate the experimental slope of the convergence curves.

solutions can only be attained with jumps of  $\varepsilon$ , this is the case analyzed. We consider an electrostatic model problem that represents a capacitor in a squared box with a dielectric material. The domain of computation is  $\Omega = [0, 1] \times [0, 1]$ , whereas the values of  $g$  in (1b) are:

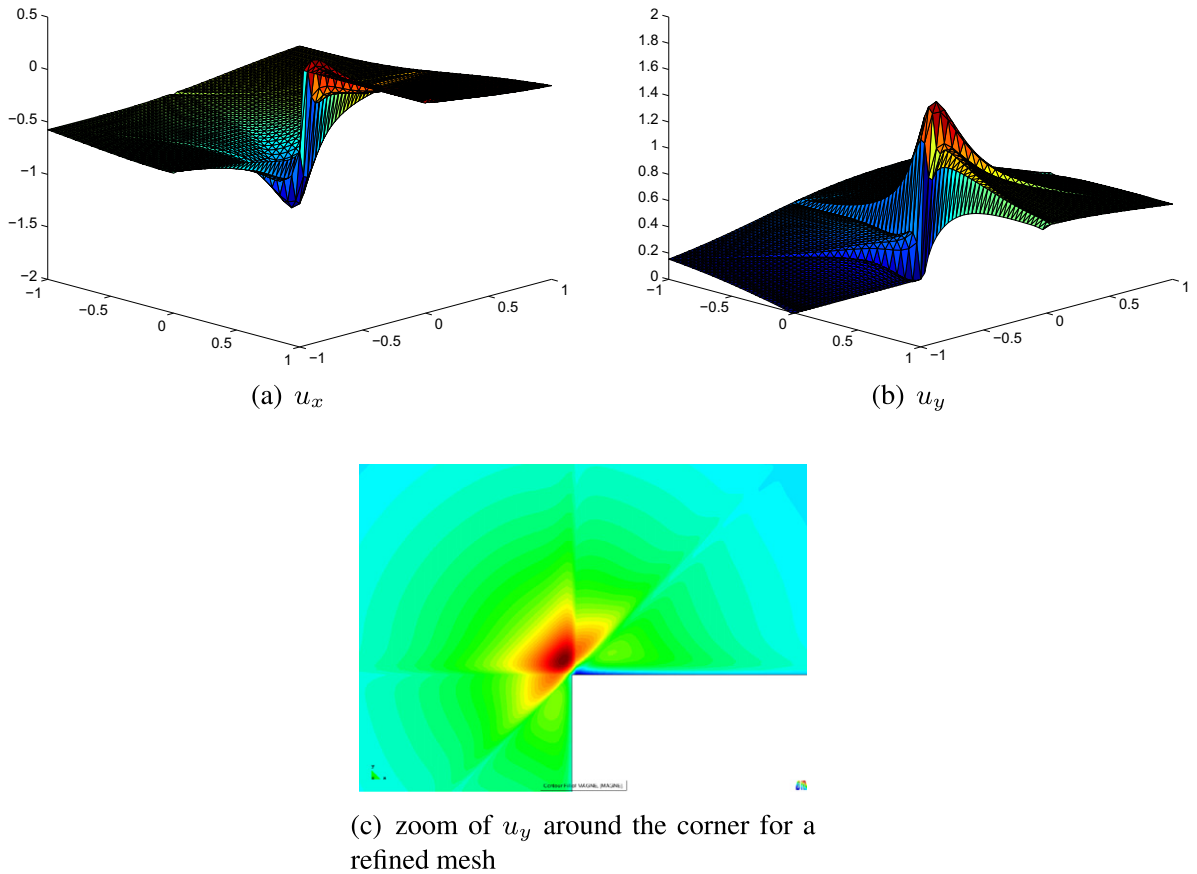


Fig. 5. Numerical solution obtained for the test problem with exact solution (35) for  $n = 1$ , for a mesh without the macro-element structure and different meshes.

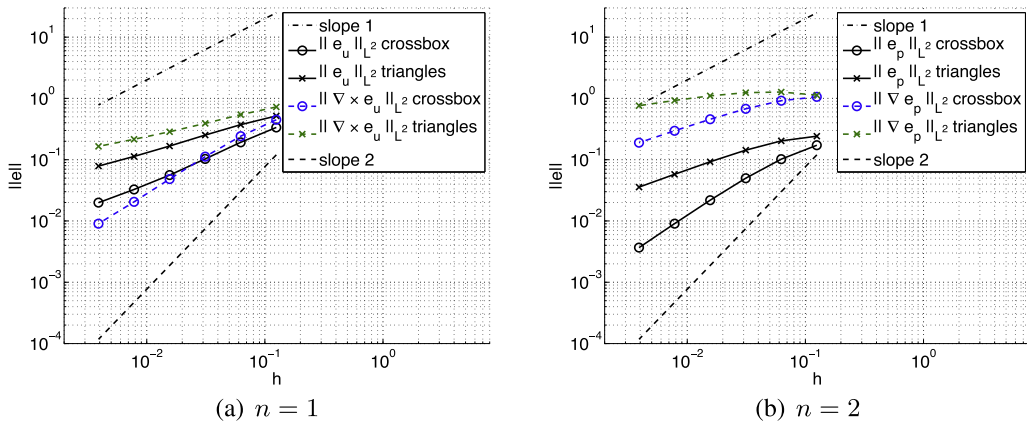


Fig. 6. Error plots for different quantities in  $L^2(\Omega)$  norm for Formulation (19)–(32) (with orthogonal projections) and the problem with analytical solution (35), for two different uniform structured meshes of triangles with/without an appropriate macro-element typology.

$$g(\mathbf{x}) = \begin{cases} +10 & \text{for } \mathbf{x} \in [0.2, 0.3] \times [0.3, 0.7], \\ -10 & \text{for } \mathbf{x} \in [0.7, 0.8] \times [0.3, 0.7], \\ 0 & \text{otherwise.} \end{cases}$$

On the other hand, we consider  $\varepsilon = \varepsilon_d$  in  $[0.4, 0.6] \times [0.3, 0.7]$ , and  $\varepsilon = 1$  on the rest of the domain. In order to satisfy the assumption that the physical parameters are constant in every patch, we have considered a partition into two patches, one for every value of  $\varepsilon$ .

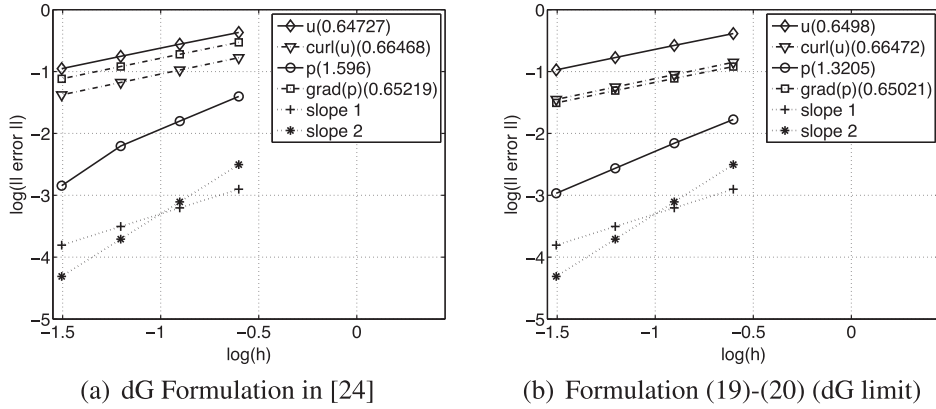


Fig. 7. Error plots for different quantities in  $L^2(\Omega)$  norm for the dG method in [24] and Formulation (19)–(20) (in the dG limit) for the test problem with analytical solution (35) and  $n = 1$ .

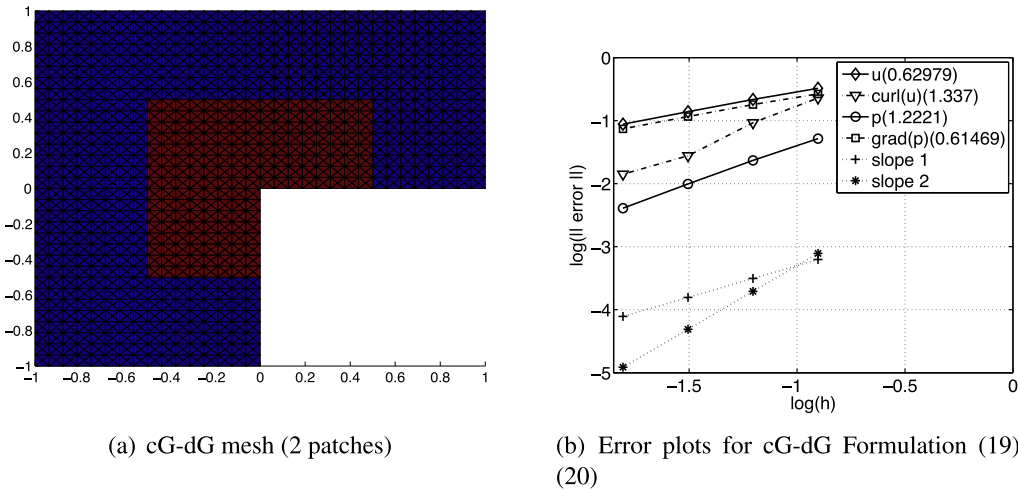


Fig. 8. Decomposition of the domain into two patches and error plots for different quantities in  $L^2(\Omega)$  norm for the cG-dG Formulation (19)–(20) for the problem with analytical solution (35) and  $n = 1$ .

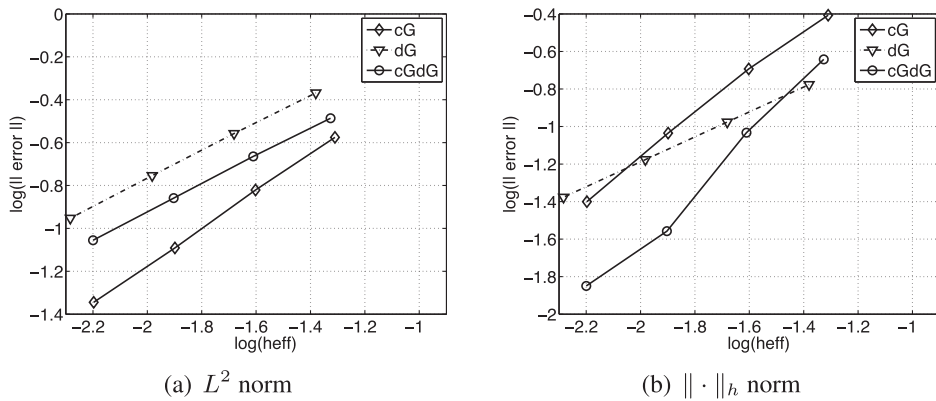
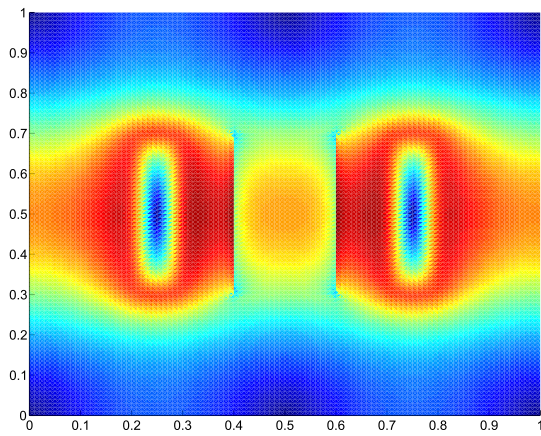
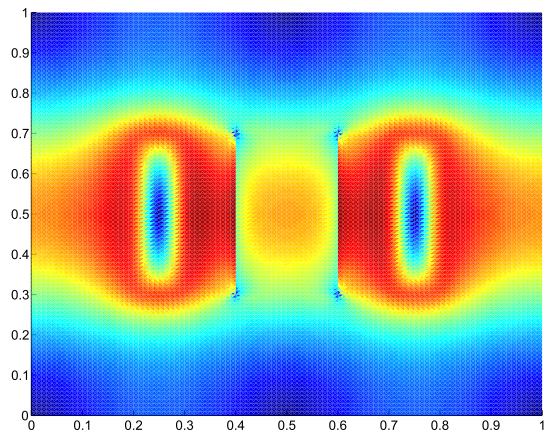


Fig. 9. Error evaluated in terms of  $\mathbf{u} - \mathbf{u}_h$  for different norms in the cG case, dG case and cG-dG case with the patches in Fig. 8(a) against the effective mesh size  $h_{\text{eff}}$ .

Let us take  $\varepsilon_d = 2$ . We show the module of  $\mathbf{u}_h$  (electric field) in Fig. 10, for the typical value of the algorithmic coefficients in the interior penalty stabilization terms, extracted from [24], as well as the results for ten times larger values of the

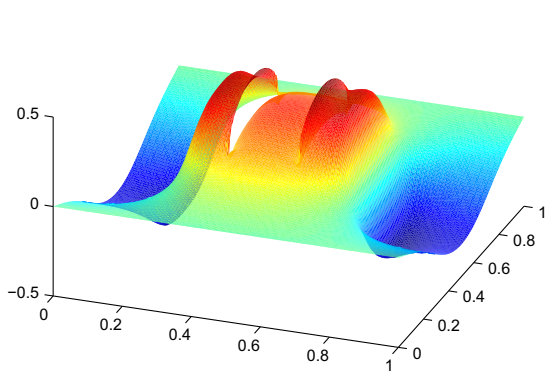


(a)  $(c_{tu}, c_{nu}, c_{np}) = (10, 1, 1)$

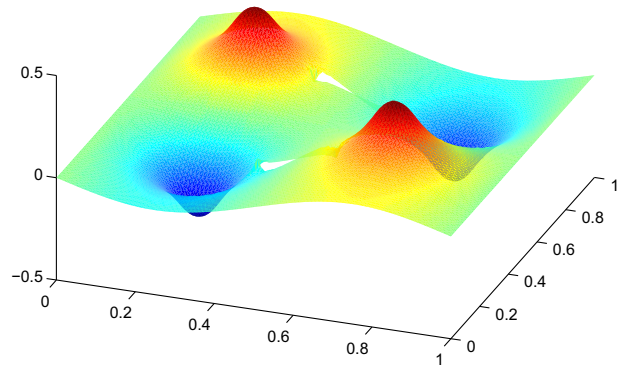


(b)  $(c_{tu}, c_{nu}, c_{np}) = (100, 10, 10)$

**Fig. 10.** Contour fills of  $|u_h|$  for  $\epsilon_d = 2$  and different values of the algorithmic constants.

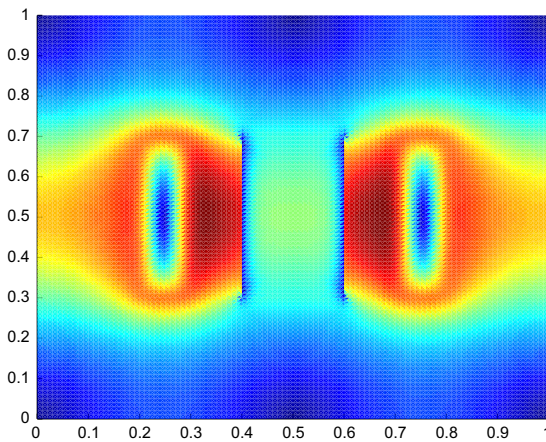


(a)  $(u_h)_x$

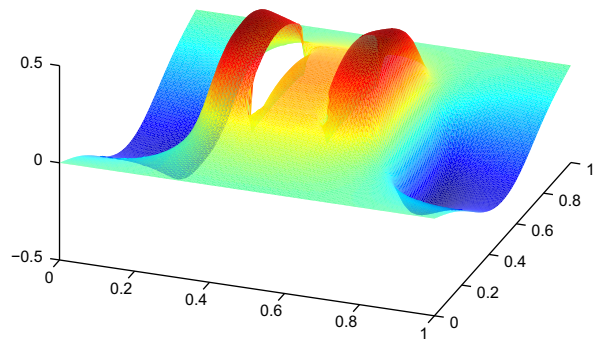


(b)  $(u_h)_y$

**Fig. 11.** Result surfaces of the components of  $u_h$  for  $\epsilon_d = 2$ .



(a)  $|u_h|$



(b)  $(u_h)_x$

**Fig. 12.** Contour fills of  $|u_h|$  and result surface of  $(u_h)_x$  for  $\epsilon_d = 10$ .

coefficients. We can see that the results are very similar, despite the clear difference in the choice of the parameters. From the numerical experiments, we have observed that the values suggested in [24] are a good lower bound. However, the formulation presented herein does not present any unstable limit as these coefficients increase, and larger values can be taken without harming the numerical computation. This cannot be done for the dG formulation in [24], where there is an upper bound for these values due to stability reasons (see Section 3.1).

In Fig. 11, we have plotted the two components of the vectorial field, in order to show the behavior of the solution at the interface between materials. In the interface sides orthogonal to the  $x$ -axis, we can see the jump of the solution, since it is  $\mathbf{n} \cdot \varepsilon \mathbf{u}$  instead of  $\mathbf{n} \cdot \mathbf{u}$  the conserved quantity. On the other hand, in those interface sides parallel to the  $x$ -axis, there is no discontinuity (despite the nodes are doubled), since  $\mathbf{n} \times \mathbf{u}$  is continuous in all cases. We can also see that the solution presents singularities on the corners of the dielectric material, as it is known from [18].

Furthermore, we have plotted the same results for a more aggressive jump of physical properties in Fig. 12, namely  $\varepsilon_d = 10$ . Clearly, the discontinuity is stronger in this case for the  $x$ -component; we have also included the contour fill of the modulus of  $\mathbf{u}_h$  in this case.

## 5. Conclusions

In this work, we have considered a numerical approximation of the Maxwell operator that allows us to use continuous and discontinuous nodal FE spaces, and so, combined spaces built from patches of continuous FE functions with discontinuities on the patch interfaces. We have denoted these three cases as cG, dG and cG–dG formulations, respectively.

The use of cG nodal FE spaces without any compatibility requirement is very appealing in terms of computational cost. Furthermore, this approach is very well suited for multi-physics problems, e.g. magnetohydrodynamics, since all the unknowns of the different subproblems can be approximated by the same FE spaces using stabilization techniques, a main difference with respect to inf–sup stable FEs (see [3]). This new approach to the Maxwell problem has been recently proposed in [4,7]. However, in electromagnetic applications that involve materials with different physical properties, cG approaches lead to large errors and wiggles on the material interfaces. For this reason, we have considered in this article a way to consider nodal cG formulations in patches, but allowing jumps on the patch interfaces. This cG–dG approach inherits the low computational cost of the cG method and is able to deal with coefficient jumps as accurately as a full dG formulation.

The combined mixed cG–dG formulation we propose combines the nodal cG formulation in [4] with the nodal dG formulation in [24] (a stabilized formulation via an interior penalty technique). In the dG limit, the first combined formulation we propose does not reduce to the dG formulation in [24]; additional terms are needed, which are not required under some inclusions, that are true for dG FE spaces using equal interpolation for both  $\mathbf{u}$  and  $p$ . Alternatively, we have motivated a new method based on orthogonal projections that does reduce the amount of element interior stabilization and recovers the formulation in [24] for the dG limit. For both formulations, stability and convergence analyses have been performed. Numerical experiments show the good behavior of the different formulations, exceeding the theoretical expectations in some cases. The experiments have been performed for a problem with a singular solution  $\mathbf{u} \notin H^1(\Omega)^d$  and another one with discontinuous physical coefficients.

## Acknowledgements

The work of the first author was funded by the European Research Council under the FP7 Programme Ideas through the Starting Grant No. 258443 - COMFUS: Computational Methods for Fusion Technology. This support is gratefully acknowledged.

## References

- [1] D.N. Arnold, F. Brezzi, B. Cockburn, L.D. Marini, Unified analysis of discontinuous Galerkin methods for elliptic problems, *SIAM Journal on Numerical Analysis* 39 (5) (2002) 1749–1779.
- [2] F. Assous, P. Ciarlet Jr., S. Labrunie, J. Segré, Numerical solution to the time-dependent Maxwell equations in axisymmetric singular domains: the singular complement method, *Journal of Computational Physics* 191 (2003) 147–176.
- [3] S. Badia, R. Codina, Stokes, Maxwell and Darcy: a single finite element approximation for three model problems. *Applied Numerical Mathematics* (2011), doi:10.1016/j.apnum.2011.07.001.
- [4] S. Badia, R. Codina, A nodal-based finite element approximation of the Maxwell problem suitable for singular solutions, UPCommons, <http://www.hdl.handle.net/2117/6064>, submitted for publication.
- [5] S. Badia, R. Codina, Unified stabilized finite element formulations for the Stokes and the Darcy problems, *SIAM Journal on Numerical Analysis* 47 (3) (2009) 1977–2000.
- [6] R. Barthelmé, P. Ciarlet Jr., E. Sonnendrücker, Generalized formulations of Maxwell's equations for numerical Vlasov-Maxwell simulations, *Mathematical Models and Methods in Applied Sciences* 17 (5) (2007) 657–680.
- [7] A. Bonito, J. Guermond, Approximation of the eigenvalue problem for the time harmonic Maxwell system by continuous Lagrange finite elements, *Mathematics of Computation* 80 (2011) 1887–1910.
- [8] S.C. Brenner, L.R. Scott, *The Mathematical Theory of Finite Element Methods*, Springer-Verlag, 1994.
- [9] F. Brezzi, M. Fortin, *Mixed and Hybrid Finite Element Methods*, Springer Verlag, 1991.
- [10] A. Buffa, P. Ciarlet Jr., E. Jamelot, Solving electromagnetic eigenvalue problems in polyhedral domains with nodal finite elements, *Numerische Mathematik* 113 (4) (2009) 497–518.
- [11] P. Ciarlet Jr., Augmented formulations for solving Maxwell equations, *Computer Methods in Applied Mechanics and Engineering* 194 (2005) 559–586.

- [12] P. Ciarlet Jr., S. Labrunie, Numerical analysis of the generalized Maxwell equations (with an elliptic correction) for charged particle simulations, *Mathematical Models and Methods in Applied Sciences* 19 (11) (2009) 1959–1994.
- [13] R. Codina, A stabilized finite element method for generalized stationary incompressible flows, *Computer Methods in Applied Mechanics and Engineering* 190 (2001) 2681–2706.
- [14] R. Codina, Analysis of a stabilized finite element approximation of the Oseen equations using orthogonal subscales, *Applied Numerical Mathematics* 58 (2008) 264–283.
- [15] M. Costabel, A coercive bilinear form for Maxwell's equations, *Journal of Mathematical Analysis and Applications* 157 (2) (1991) 527–541.
- [16] M. Costabel, M. Dauge, Singularities of electromagnetic fields in polyhedral domains, *Journal of Mathematical Analysis and Applications* 151 (3) (2000) 221–276.
- [17] M. Costabel, M. Dauge, Weighted regularization of Maxwell equations in polyhedral domains, *Archives for Rational Mechanics and Analysis* 93 (2) (2002) 239–277.
- [18] M. Costabel, M. Dauge, S. Nicaise, Singularities of Maxwell interface problems, *M2AN Mathematical Modelling and Numerical Analysis* 33 (1998) 627–649.
- [19] H.Y. Duan, F. Jia, P. Lin, R.C.E. Tan, The local  $L^2$  projected  $C^0$  finite element method for Maxwell problem, *SIAM Journal on Numerical Analysis* 47 (2) (2009) 1274–1303.
- [20] A. Ern, J.L. Guermond, *Theory and Practice of Finite Elements*, Springer-Verlag, 2004.
- [21] P. Fernandes, G. Gilardi, Magnetostatic and electrostatic problems in inhomogeneous anisotropic media with irregular boundary and mixed boundary conditions, *Mathematical Models and Methods in Applied Sciences* 7 (1997) 957–991.
- [22] C. Hazard, Numerical simulation of corner singularities: a paradox in Maxwell-like problems, *Comptes Rendus-Mécanique* 330 (1) (2002) 57–68.
- [23] C. Hazard, M. Lenoir, On the solution of time-harmonic scattering problems for Maxwell's equations, *SIAM Journal on Mathematical Analysis* 27 (6) (1996) 1597–1630.
- [24] P. Houston, I. Perugia, D. Schötzau, Mixed discontinuous Galerkin approximation of the Maxwell operator, *SIAM Journal on Numerical Analysis* 42 (1) (2005) 434–459.
- [25] T.J.R. Hughes, Multiscale phenomena: Green's function, the Dirichlet-to-Neumann formulation, subgrid scale models, bubbles and the origins of stabilized formulations, *Computer Methods in Applied Mechanics and Engineering* 127 (1995) 387–401.
- [26] R. Liu, M.F. Wheeler, C.N. Dawson, R.H. Dean, On a coupled discontinuous/continuous Galerkin framework and an adaptive penalty scheme for poroelasticity problems, *Computer Methods in Applied Mechanics and Engineering* 198 (2009) 3499–3510.
- [27] I. Perugia, D. Schötzau, P. Monk, Stabilized interior penalty methods for the time-harmonic Maxwell equations, *Computer Methods in Applied Mechanics and Engineering* 191 (2002) 4675–4697.
- [28] D. Schötzau, Mixed finite element methods for stationary incompressible magneto-hydrodynamics, *Numerische Mathematik* 96 (2004) 771–800.